DAΦNE TECHNICAL NOTE

INFN - LNF, Accelerator Division

Frascati, April 12, 2001

Note: **BM-7**

(Submitted to Nuclear Instruments and Methods in Physics Research: Section A)

Single Bremsstrahlung Luminosity Measurements at DAΦNE

G. Mazzitelli[1], F. Sannibale[1], F. Cervelli[2], T. Lomtadze[2], M. Serio[1], G. Vignola[1]

[1]INFN Laboratori Nazionali di Frascati - C.P. 13 00044 Frascati – Italy

[2]INFN Sezione di Pisa - C.P. 56010 San Piero a Grado (PI)- Italy

Abstract

At DAΦNE luminosity measurements are performed by detecting Single Bremsstrahlung at the two interaction points. Set-up and measurement method are presented with special emphasis on background subtraction schemes, error evaluation and machine related issues.

1. Introduction

DAΦNE, the Frascati phi-factory [1], is a 510+510 MeV electron-positron collider, tuned on the Φ meson resonance and mainly devoted to the study of CP violation in the Kaon decay. In order to optimize operationally the luminosity performance, the related machines parameters must be accurately set relying on a tuning process [2, 3] based on the readout of a luminosity monitor. In designing such a monitor the following major requirements were pursued: i) capability of performing very fast measurements to allow machine parameters tuning in real time, ii) measurement stability with respect to variations of the beam position and angle at the interaction point (IP), iii) no interference with the experiments to ensure independent luminosity measurements during the data taking and during the initial phase of the machine commissioning with no experiment installed in the two interaction regions (IR).

A direct way to measure luminosity consists in measuring the counting rate of a known electromagnetic process while the beams are colliding. Good candidates are small angle *bhabha scattering* (BB), *single bremsstrahlung* (SB) and *double bremsstrahlung* (DB). Differential and integrated cross-sections for BB, DB and SB are reported in references [5, 6, 7]; an interesting comparison among measurements with the three different processes can be found in reference [8]. At DAΦNE SB was chosen because it better fulfills requirements i) and ii) [4] and ensures measurements at a few percent level when an efficient background subtraction method is used.

2. Single bremsstrahlung luminosity measurement method

2 1. Method description

In SB process

$$e^+ + e^- \rightarrow e^+ + e^- + \gamma \tag{1}$$

photons are emitted with cylindrical symmetry with respect to the beam particle trajectory at IP within a cone of total aperture ~ E_{rmu}^{-1}, where E_{rmu} is the beam particle energy expressed in electron rest mass units (in DAΦNE E_{rmu} = 999). The maximum energy $k_{\max}$ the photons can have is [7]:

$$k_{\max} = \frac{\omega}{2} - \frac{m_o^2 c^4}{2\omega} \cong \frac{\omega}{2} \tag{2}$$

where ω is the center of mass energy of the colliding beams (twice the energy of the single beam in DAΦNE), m_0 is the electron rest mass and c is the speed of light.

If the energy and the rate $\dot{N}_{SB}$ of photons are measured by a proportional counter, then the luminosity value L can be evaluated:

$$L = \dot{N}_{SB} \Big/ \zeta_{SB}(k_T, \Omega_D) \tag{3}$$

with ζ_{SB} the SB integrated cross-section

$$\zeta_{SB}(k_T, \Omega_D) = \int_{k_T}^{k_{\max}} dk \int_{\Omega_D} d\overline{\Omega} \frac{\partial^3 \zeta_{SB}}{\partial k \, \partial \overline{\Omega}} \tag{4}$$

Ω_D the portion of solid angle viewed by the photon detector and k_T the minimum photon energy that can be detected. The measurement system must allow to choose the proper value of this threshold k_T permitting either to cut the low energy part of the photon spectrum where the background due to undesired processes is large, either to select the average counting rate that the monitor electronics can properly handle.

Some considerations concerning the quantities in (3) and (4) are in order. Helpful expressions for the differential and integral SB cross-sections to be used in some typical cases are reported in Appendix A. The counting rate $\dot{N}_{SB}$ is a measured quantity, $k_{\max}$ can be calculated by (2) and Ω_D is defined by the geometry of the interaction region and of the photon detector: typically a collimator, with a circular aperture, is placed in front of the detector in order to make the Ω_D evaluation simpler. The threshold k_T is typically the result of a pulse height discrimination process. As the chain that transforms the collected photon energy into an electrical signal is generally complex, the evaluation k_T is difficult and a calibration procedure is necessary.

2. 2. Energy threshold calibration by gas bremsstrahlung

The following calibration technique is based on the *gas bremsstrahlung* process (GB), where a gamma photon is emitted when a beam particle interacts with a molecule of the residual gas inside the accelerator vacuum chamber. The GB properties are theoretically well known [9]: similarly to the SB case, the maximum energy that a photon can assume is $\omega/2$ and the total angular aperture of the emission cone is $\sim E_{rmu}^{-1}$. For these reasons, the same experimental set-up for SB can be directly used for detecting the GB photons and for measuring their energy spectrum. On the other hand, an analytical expression for the GB spectrum can be obtained by convoluting the theoretical GB cross-section with the detector resolution function (DRF) (see Appendix B). Thus, by comparing the theoretical and experimental spectra the measurement calibration can be achieved. A complete description of the calibration process is reported in [8]; hereafter only the essential issues are described. In the process it is used the so-called *modified spectrum* that is obtained by multiplying the energy differential GB cross-section by the photon energy. Figure 1 shows the theoretical modified spectra for different calorimeter resolutions. In the plot, the photon energy has been expressed in $k_{\max}$ units and $k_T = 0.2\ k_{\max}$. In the experimental setup, the signal of the proportional counter (calorimeter) is typically digitized by an ADC (see section 3.3), so that the sampled modified spectra will have the ADC channel number in abscissa and the number of photon counts multiplied by the channel number in ordinate. These experimental abscissa and ordinate will be indicated with *x* and *y* respectively. The final aim of the procedure is to calibrate the abscissa variable *x*. It has been demonstrated [8] that, in the case of a gaussian DRF with arbitrary standard deviation, the ordinate $y_{\max}$ of the modified spectrum corresponding to $k_{\max}$, see Figure 1, is always given by:

$$y_{\max} = y_P \big/ 1.82 \qquad \Delta y_{\max} \big/ y_{\max} = \pm 0.013 \tag{5}$$

where y_P is the ordinate of the spectrum flat region (zero derivative point). By measuring y_P on the experimental spectrum, $y_{\max}$ can be evaluated by expression (5) and the $k_{\max}$ experimental abscissa $x_{\max}$ can be localized. Another quantity to be individuated in the experimental spectrum is the position x_0 on the abscissa corresponding to $k = 0$. This can be done, by simply measuring the x_0 value when no pulse from the detector is present or by a more sophisticated technique explained in section 4.1.2. At this point, if the monitor electronics response is linear, the calibration function is completely defined:

$$k = \frac{k_{\max}}{x_{\max} - x_0}\left(x - x_0\right) \tag{6}$$

and using in expression (6) the threshold position , measured in the experimental spectrum, k_T can be finally evaluated.

In order to avoid contamination of the GB spectrum due to SB photons, the calibration must be performed with non-colliding beams (preferably with only one beam stored). Another important source of contamination is the background induced by particles lost by the beam.

This contribution can be strongly reduced by properly shielding the detector and performing the calibration procedure in a situation of good beam lifetime. Obviously the part of the detector facing the IP and receiving the 'good' GB photons cannot be shielded and the background impinging on that part will generate spurious counts. The charged part of this residual background can be efficiently eliminated by a clearing field in front of the detector and by using as veto the signal from a (thin) scintillator system (sensitive to charged particles only) placed in front of the detector. Finally, the contribution of the residual background photons, that statistically have lower energies than the GB ones, can be partially reduced by increasing the value of the threshold k_T.

In DAΦNE, even at very low values of stored current the GB counting rate is already > 10 kHz, so the cosmic ray contribution, few hertz, can always be neglected.

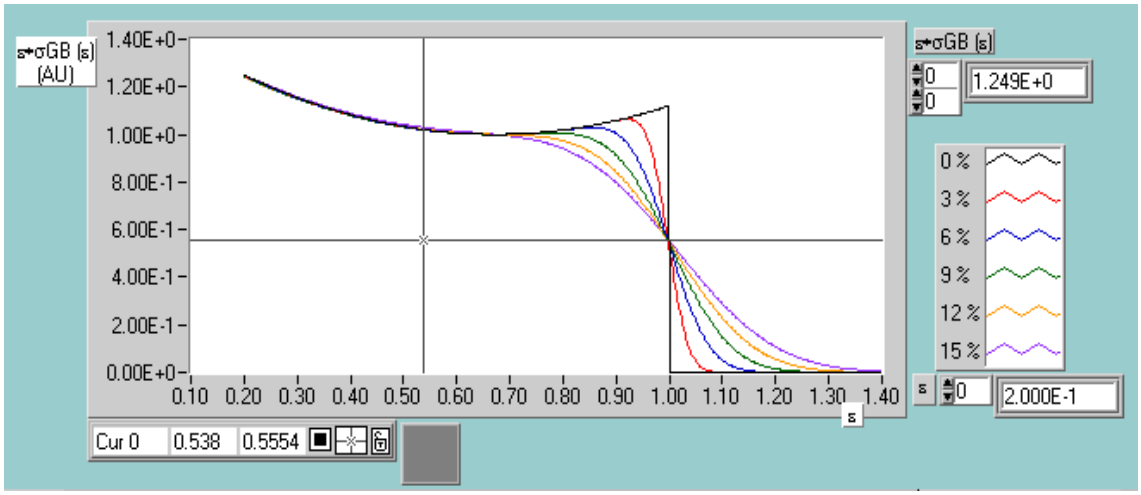

Figure 1: Gas bremsstrahlung theoretical cross-section times normalized energy vs. normalized energy. The different curves are for different calorimeter resolutions. The step-like function indicates the case of an ideal calorimeter with zero resolution.

2. 3. Background and background subtraction schemes

In DAΦNE the luminosity monitor is extensively used as a tool for the tuning of the machine parameters for luminosity performance (see section 5.3). In such a mode of operation only relative measurements are required and no background subtraction is necessary. On the contrary when absolute measurements are requested background must be accurately removed.

The same GB process used for calibration is the main source of background during an absolute luminosity measurement. The measured rate $\dot{N}_M$ with the beams in collision is the result of three main contributions:

$$\dot{N}_M = \dot{N}_{SB} + \dot{N}_{GB} + \dot{N}_{dI} \qquad (7)$$

where $\dot{N}_{SB}$ is the term due to SB, $\dot{N}_{GB}$is due GB and $\dot{N}_{dI}$ is a term that depends on the stored beam losses. In DAΦNE the contributions due to double bremsstrahlung and to cosmic rays are negligible (see section 4.1.4).

The term $\dot{N}_{GB}$ is proportional to the average residual gas pressure p_{IR} at the IR and to the average current of the beam viewed by the detector. If, for example, the detector is collecting the photons produced by the positron beam:

$$\dot{N}_{GB} = \alpha\, p_{IR} I_{+} \tag{8}$$

where I_{+} is the stored positron current and α is the proportionality constant.

The pressure p_{IR} can be written as:

$$p_{IR} = p_0 + \beta_{+} I_{+} + \beta_{-} I_{-} \tag{9}$$

where I_{-} is the stored electron current, p_0 is the pressure at IR when no beam is stored and β_{+} and β_{-} are the quantities describing the pressure contribution due to the gas desorption induced in the vacuum chamber by the synchrotron light of the two beams. By merging (9) in (8):

$$\dot{N}_{GB} = \alpha\beta_{+} I_{+}^2 + \alpha p_0 I_{+} + \alpha\beta_{-} I_{+} I_{-} \tag{10}$$

Measuring $\dot{N}_{GB}$ at different values of I_{+} and I_{-} and fitting the data by the expression (10) it is possible obtaining p_0, α, β_{+} and β_{-}. Actually these parameters present a slow dependence on time. The pressure p_0 progressively changes under the vacuum system pumping action and because of the vacuum conditioning induced by the beam synchrotron radiation. The parameter α, which depends on the average quadratic value of the atomic number of the residual gas, also changes under the action of the pumping system that has different efficiencies for different gases and therefore modifies the residual gas composition. Moreover the β quantities, progressively decreases under the cleaning action of the synchrotron light on the vacuum chamber. Additionally, in expression (10) the effects induced in multibunch operation by different filling patterns of the stored beams are not included. In fact, while the average value of the stored current determines the average power that the synchrotron radiation releases on the vacuum chamber, the multibunch filling pattern determines the peak value of that power. Thus the same current stored with different patterns, may generate different vacuum chamber temperature configurations with different thermal outgassing rates and pressures. All the mentioned reasons make the use of the expression (10) impractical.

The last contribution in (7), $\dot{N}_{dI}$, is generated by beam losses reaching directly the luminosity detector or producing on the vacuum chamber secondaries that arrive up to the detector. The evaluation of this background is quite difficult because its production process depends on many factors including, for example, the phenomenon generating the particle loss (gas scattering, Touschek effect, beam-beam effects, etc.), the closed orbit, the machine optical functions and the dynamic pressure value. Anyway, the same arrangements and solutions adopted for reducing the background during the GB calibration described in section 2.2 are effective in maintaining the $\dot{N}_{dI}$ contribution negligible during the luminosity measurement.

Being a reliable evaluation of the background very difficult, two different schemes were adopted to remove the background during the measurement. In both of them the contribution of $\dot{N}_{dI}$ must be negligible.

The first one, that will be called *Separate Beams Background Subtraction* (SBBS) consists in making the difference between the counting rates obtained bringing the beams in and out of collision. The beams can be separated at the IP by different techniques but, for all of them, in order to obtain a good separation at the IP some conditions must be carefully fulfilled. First of all, for avoiding collisions between the beam tails, which could bring to an overestimate of the background, the beams must be separated from each other by several sigmas (beam r.m.s. dimension). Second, the separation, as well as any orbit variation, must be absolutely performed by moving only and exclusively the beam that does not point the luminosity detector. In fact, if the other beam is moved, the GB source can change in position, shape and thickness inducing strong variations on the counting rate. Last but not least, the separating procedure must not generate any beam loss.

Of course, the separation can be horizontal, vertical or longitudinal. In DAΦNE the flat beams and the horizontal crossing angle at IP make difficult to obtain an effective horizontal separation. On the contrary in the vertical plane a separation of ~ 200 sigmas or more (one vertical sigma is ~ 20 μm) can be achieved by applying on both the beams a closed bump at the IR. Longitudinal separation is possible only in those colliders, such DAΦNE, with separate rings and RF cavities where it can be easily obtained by changing the phase of one or both the ring RF's.

In high luminosity machines with a low beta scheme at IR, additional care must be taken in separating the beams. In such a configuration the derivative of the vertical beta function with respect to the distance from the IP is very steep and a point at a relatively small distance from the IP will have optical functions significantly different than those at the IP. This situation can have a strong effect when the separation is removed and the beams are brought in collision. In fact, if during the transition the beams collide with a different IP configuration, than the beam-beam effects are not controlled and can generate losses in the stored beams. To have relevant effects, this scenario must repeat itself during several turns and thus a good way to efficiently reduce and even eliminate the effect is to make the transition time as short as possible. This is not always possible, in DAΦNE, for example, the vertical separation is obtained performing a bump at IR by means of corrector magnets external to the aluminum vacuum chamber. Because of the eddy currents on the chamber, a transition shorter than ~ 10 ms is practically not achievable and with a revolution period of about 300 ns the bump cannot be removed or applied in less than $3\ 10^4$ turns. In such a situation, the transient effect can be still avoided if the magnets power supplies are properly driven in order to scale the bump without deformation, maintaining during the transition, the same IP configuration. Fast transitions can be instead obtained if the separation is longitudinal. In DAΦNE, where it is used what we have called the *phase jump* technique, the positron beam is injected 360, 540 or 720 RF degrees far from the collision and then brought in collision with a fast phase variation to 0° in about ten synchrotron periods $\left(f_{sync.} \approx 30\ kHz\right)$. The technique can be used in both single and multibunch operation modes and the small amplitude synchrotron oscillation, which is excited during the transition, very quickly damps to zero [10]. In this longitudinal separation scheme it is preferable to have the beams separated enough in order to avoid parasitic crossing during the injection. In fact, if the longitudinal separation is not sufficient, the large horizontal betatron

oscillations during the injection transient can force the injected beam into collision with the stored one, with possible limitations on the injection. In DAΦNE, which has 120 buckets per ring, the phase jump scheme is obviously limited to 60 bunches maximum. For the 120 bunches configuration a vertical separation scheme is still necessary.

$\dot{N}_{GB}$ and $\dot{N}_{SB}$ have a different dependence on the beam currents. In fact $\dot{N}_{SB}$ scales with the product of the currents of the colliding beams, while $\dot{N}_{GB}$ scales according to expression (10). This situation implies that, when the SBBS scheme is used, it is necessary to periodically separate the beams for updating the background value. This is not necessary when the second method of background subtraction is used. The *Missing Bunch Background Subtraction* (MBBS) is a variation of the method described in reference [8]. In DAΦNE the following configuration has been adopted. A single bunch is injected and stored into the electron ring. Two bunches are instead injected into the positron ring, one in the bucket colliding with the stored electron bunch and the other one in a bucket not in collision. Assuming that the residual gas pressure does not change between the passage of the two positron bunches and assuming that the background is due to the GB contribution only, it is possible to write using expressions (7) and (8):

$$\dot{N}_C = \dot{N}_{SB} + \alpha p_{IR} I_C^+ \tag{11}$$

$$\dot{N}_{NC} = \alpha p_{IR} I_{NC}^+ \tag{12}$$

where $\dot{N}_C$ and $\dot{N}_{NC}$ are the counting rates relative to the colliding and non-colliding bunches respectively, $\dot{N}_{SB}$ is the counting rate due to SB photons and I_C^+ and I_{NC}^+ are the currents of the colliding and non-colliding positron bunches. It is direct to derive from expressions (11) and (12) the relation:

$$\dot{N}_{SB} = \dot{N}_C - \frac{I_C^+}{I_{NC}^+} \dot{N}_{NC} \tag{13}$$

Thus if the luminosity monitor electronics allows to discriminate the counts from different bunches, then by measuring the current ratio of the positron bunches, it is possible, by expression (13), to remove the GB background and to evaluate the SB counting rate. The current ratio can be obtained in two different ways: by a bunch by bunch current monitor that continuously measures and updates the ratio value or by sampling the GB produced by the two bunches in a point where the beams are not in collision. In fact, according to (8), the ratio of the GB counting rates is equal, in this situation, to the ratio of the currents. The MBBS method as described allows luminosity measurements in the case where only one bunch per beam is in collision. Anyway it can be directly generalized to multibunch mode if the collider is filled in such a way that, in one ring, all the bunches except one (or a few) have the colliding partner in the other ring. In this case expression (13) is still valid under the condition that all the terms must now be intended as the sum of the contributions of every single bunch, so I_C^+ will be the sum of the currents of all the positron bunches under collision, $\dot{N}_{NC}$ the sum of the counting rates relative to all the positron bunches not in collision and so on.

It is important to remark that in both the presented background subtraction schemes it is assumed that thickness and position of the GB source do not change between the in and out of collision situations. In fact, any phenomenon, that changes the position or the angle at IP of the beam pointing the calorimeter, will generate a modification of the GB target with a consequent variation in the background counting rate. For example, the possible effects of a residual beam-beam deflection must be controlled.

3. The DAΦNE SB luminosity monitor

3. 1. Interaction region layout

The positron and electron beams in DAΦNE are stored in 2 (~100 m long) independent rings with separated vacuum chambers. Only at the 2 IR's, ~ 10 m long, the beams share a common chamber. A horizontal splitter magnet, placed at each of the IR's extremes, allows combining and separating the beams in the single to separated chamber transition. The beams collide at IP with a half horizontal crossing angle of 12.5 mrad, tunable from 10 to 15 mrad. Figure 2 shows the splitter area with the position of the proportional counter of the luminosity monitor. The layout allows placing a counter in proximity of each of the IR splitters from the separate chambers side.

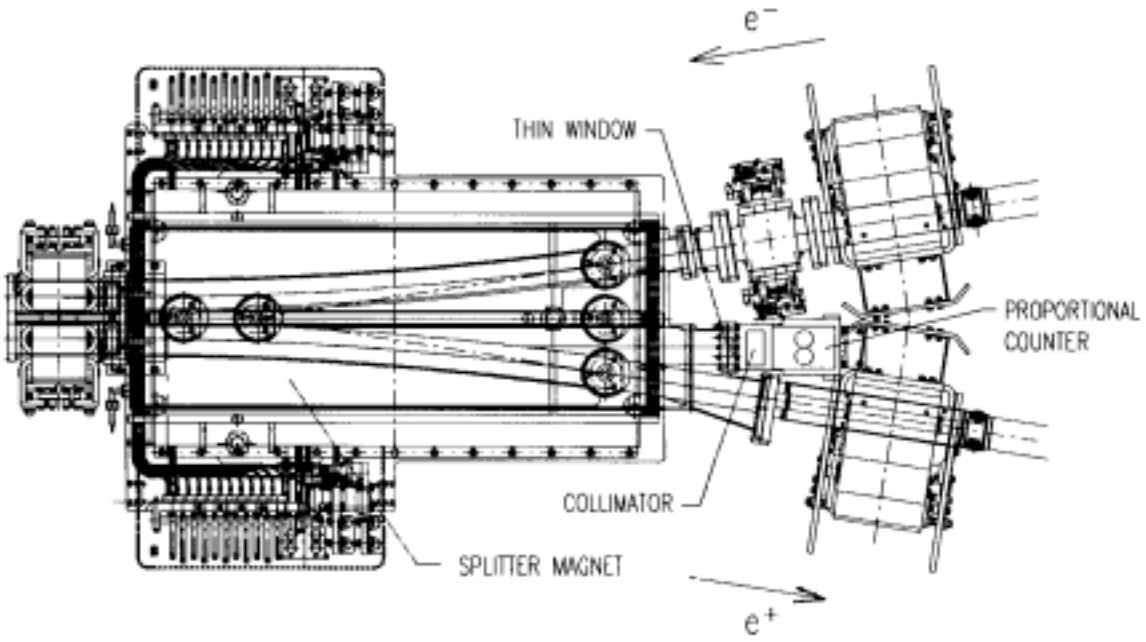

Figure 2: Single bremsstrahlung luminosity monitor layout at splitter magnet area.

A total number of two calorimeters have been built and they can be placed or moved from one IP to the other according to the needs of the moment. At the present time both of them are installed in the KLOE experiment IR, one pointing the positrons and the other pointing the electrons. In this way two independent luminosity measurements can be simultaneously performed. The distance between the detector and the IP is ~ 6 m. At the splitter output, a thin aluminum window, 1.5 mm thick, allows the gamma photons to come out the vacuum chamber and to arrive to the detector. Between the thin window and the proportional counter a 10 radiation length lead collimator with a 10 mm radius circular aperture can be inserted to force the shape of the accepted solid angle Ω_D to a cone of 1.6 mrad semi-aperture centered on the crossing angle of 12.5 mrad. The integration of the SB cross section within this solid angle indicates that, in this configuration, about 70% of the SB gamma photons are accepted (see section 4.1.3).

3. 2. Proportional Counter

The proportional counter is a lead-scintillating fiber calorimeter with photomultiplier (PMT) read-out. The sampling structure is the same as the one of the KLOE electromagnetic calorimeter [11].

The calorimetric module is built up by gluing 1 mm diameter green-blue scintillating fibers between thin grooved lead plates, obtained by passing 0.5 mm thick lead foils through rollers of proper shape. The grooves in the two sides of the lead are displaced by one half of the pitch so that fibers are located at the corners of adjacent, quasi-equilateral triangles resulting in optimal uniformity of the final stack. The grooves are just deep enough to insure that the lead does not apply direct pressure on the fibers. The blue-green scintillating fibers (Pol.Hi.Tech-46) provide high light yield, short scintillation decay time and long attenuation length [12]. The selected fiber pitch of 1.35 mm results in a structure which has a fiber:lead:glue volume ratio of 48:42:10 and a sampling fraction of ~ 15% for a minimum ionizing particle. The final composite has a density of ~ 5 g/cm^3 and a radiation length of ~ 1.6 cm, it is self-supporting and can be easily machined. The resulting structure is quasi-homogeneous and has high efficiency for low energy photons.

This kind of sampling calorimeter has been extensively tested [13] presenting an excellent linearity and resulting to have an energy resolution for fully contained electromagnetic showers induced by photon, given by:

$$\frac{\sigma_E}{E} = \frac{4.4\%}{\sqrt{E_{(GeV)}}} \qquad (14)$$

The luminosity monitor calorimeter has a squared face ($122 \cdot 122$ mm^2) and is 184 mm long, corresponding to 11.5 radiation lengths. Fibers are vertically positioned and the light is collected on the topside by a plastic light guide tapered in order to match the calorimeter and the photomultiplier area.

In front of the calorimeter a 5 mm thick fluorine doped polystyrene scintillator is placed for detecting the charged particles produced by the electromagnetic showers in the lead collimator. The splitter magnet field acts as a very efficient clearing field for the particles coming from the IP (bhabha's, beam lost particles). Finally lead shields are placed all around the detector for minimizing spurious counts due to particles and gamma photons hitting the lateral and back faces of the detector.

Because of the configuration of the splitter area we were forced to place the calorimeter in a region immersed into the fringe fields of the near magnets. The intensity of these fields (80 gauss max.) is not sufficient for creating problems to the lead-fiber structure of the calorimeter but it is instead large enough to inhibit the correct operation of most photomultipliers. In DAΦNE two actions were adopted for efficiently removing the problem. In first place the plastic light guide between the calorimeter and the photomultiplier was built long enough to bring the tube into a < 20 gauss region, secondly a photomultiplier compatible with the presence of magnetic fields was used (Hamamatsu H6155-01 - 3 inches diameter). With this arrangement the problem has been practically eliminated, in fact no measurable variation of the calorimeter counting rate has been observed while changing the field intensities of the near magnets.

A single photomultiplier with wide area has been used because this choice relevantly simplifies the monitor calibration. In fact, a multi-tube configuration requires a careful and very difficult equalization of the photomultiplier gains, which is of course not necessary in the single tube case.

3. 3. Photon energy analysis and counting system

The luminosity monitor electronic systems, one for each of the luminosity calorimeters, are located ~ 50 m far away from the calorimeters in an external experimental area outside the DAΦNE rings hall. Figure 3 shows the block diagram of the single system. It can be divided in two main parts, the *digital channel* for the measurement of the counting rate and the *analog channel* where the gamma photons energy analysis is performed during the acquisition of the GB spectra in the calibration process. With reference to Figure 3, the signal coming from the calorimeter photomultiplier arrives to an analog fan out that splits the signal into two different paths. In the digital channel a discriminator generates a NIM trigger every time the detector signal height is larger than a software specified threshold. An anticoincidence, between the trigger and the signal generated by the scintillator in front of the calorimeter, can be activated for eliminating, as previously described, spurious counts due to charged particles. Similarly, the coincidences between the trigger and two selectable bunches (or group of bunches), that are necessary in the MBBS technique described in section 2.3, can be also activated. These filtered triggers are finally sent to a scaler for the counting rate acquisition and to the GATE input of a charge integrating ADC used in the analog channel where the other part of the signal coming from the calorimeter is integrated and acquired for the energy spectrum analysis described in section 2.2. A test signal, variable in charge, can be generated at the electronics input for testing the system linearity.

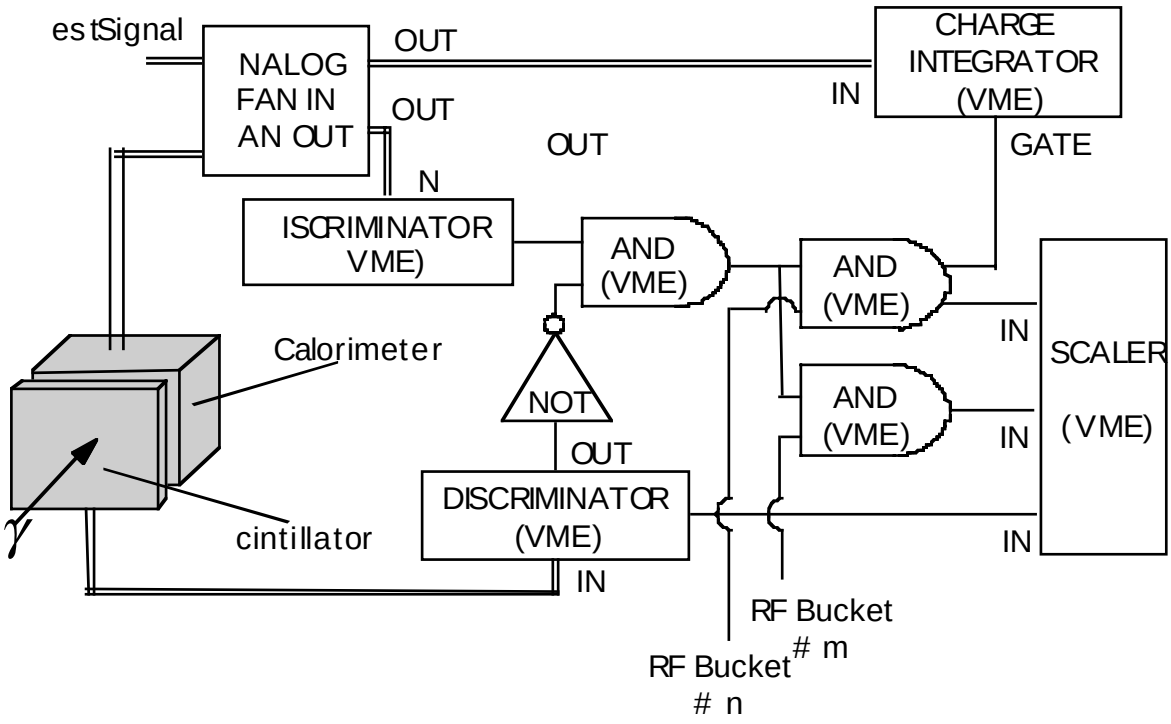

Figure 3: Photon energy analysis and counting system electronics block diagram.

All the system components that need to be remotely controlled, are in VME standard and are directly integrated in the DAΦNE control system [14]. All the remaining components are in NIM standard. The photomultiplier HV power supplies (ISEG VHQ 203M), the discriminator (CAEN V258), the scaler (STRUCK STR7200) and the charge integrating ADC (CAEN V265N) belong to the first category while the analogic fan out (LNF design), the logic units (PHILLIPS SCIENTIFIC 752) and the delay units used for the system timing (EG&G-ESN DV8000) belong to the second group.

All the digital triggers are NIM standard signals with ~ 50 ns FWHM. This configuration limits the system bandwidth (BW) to 18 MHz (measured value). BW can be increased by decreasing the trigger width. In the present configuration a lower limit of 20 ns FWHM (BW 40 MHz) exists due to the photomultiplier signal width. The implications of BW on the measurement error will be discussed in section 4.1.1. The maximum sampling rate of the analog channel is ~ 1 kHz.

The monitor software is fully integrated in the DAΦNE control system and is written in LabView. It allows the control of all the settings necessary for the proper operation and calibration of the monitor. Figure 4 shows the main control window during a typical luminosity run.

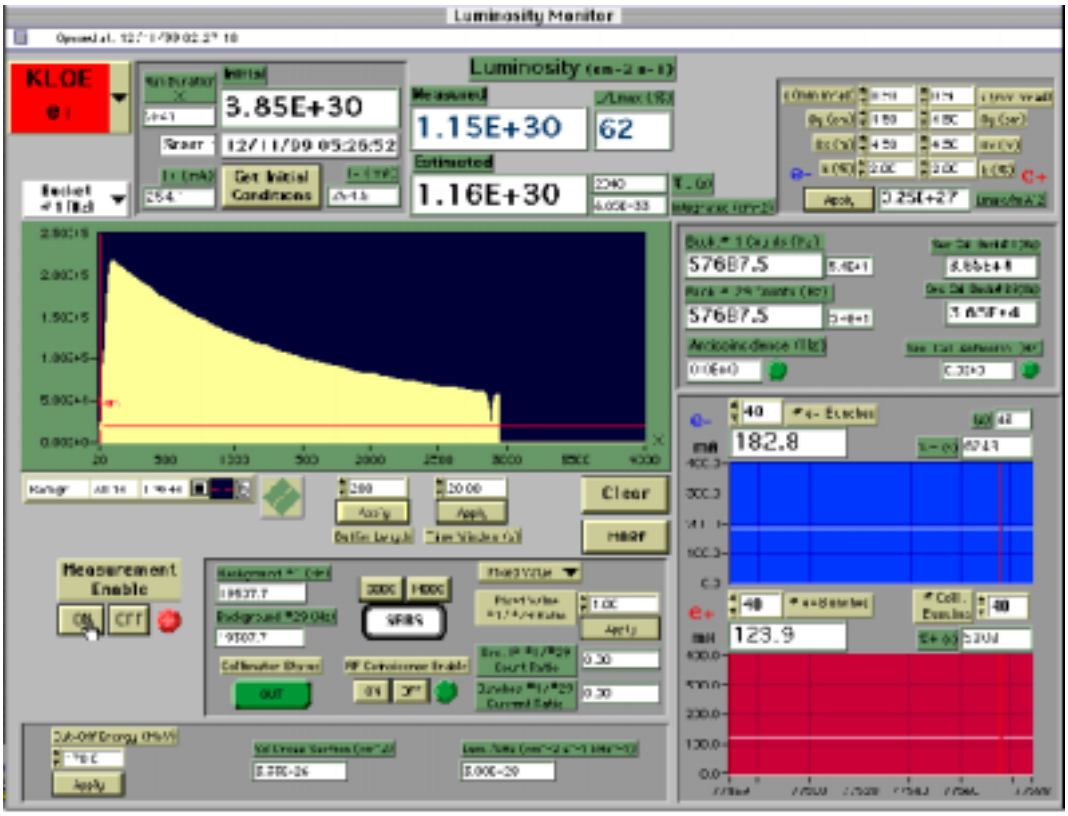

Figure 4: Luminosity monitor main control window.

4. Error analysis

4.1. Systematic Errors

4.1.1 Accidentals

Accidental counts introduce a systematic error in the luminosity measurement. The situation in the single colliding bunch mode of operation will be first considered.

Let p the average probability that a particle of the electron bunch undergoes a SB scattering (that can be detected by the monitor calorimeter) with a particle of the counter-rotating positron bunch during a single passage at IP. In the case of gaussian transverse distributions $p = \zeta_{SB} / 4\pi\sigma_x^*\sigma_y^*$, being σ_x^* and σ_y^* the rms horizontal and vertical beam sizes at the IP. The probability of SB events per electron per single passage is then given by $N_+ p$, while the average number of SB events per passage is $N_- N_+ p$ (N_- and N_+ are respectively the number of positrons and electrons per bunch). If f_R is the revolution frequency then the SB counting rate $\dot{N}_{SB}$ is given by:

$$\dot{N}_{SB} = N_- N_+ p f_R \qquad (15)$$

The probability of a simultaneous SB event of two electrons in a single passage is $(N_+ p)^2$. The counting rate $\dot{N}_{SB}^{Ac}$ of accidentals (events with two SB per crossing) is therefore given by:

$$\dot{N}_{SB}^{Ac} = \binom{N_-}{2}(N_+ p)^2 f_R = \frac{N_-(N_- - 1)}{2}(N_+ p)^2 f_R \cong \frac{(N_- N_+ p)^2}{2} f_R \qquad (16)$$

Analogously, the counting rate due to triple SB events is equal to $(N_- N_+ p)^3 f_R / 6$. It follows that situations with more than two simultaneous events can be neglected as far as $N_- N_+ p/3$ is a small number. In DAΦNE $p \approx 4 \cdot 10^{-24}$ and $N_\pm < 9 \cdot 10^{10}$ so that $N_- N_+ p/3 \cong 1 \cdot 10^{-2}$ allowing to consider only double events.

The ratio *R* between accidentals and SB counting rates can be written by expressions (15) and (16) as:

$$R = \frac{\dot{N}_{SB}^{Ac}}{\dot{N}_{SB}} = \frac{N_+(N_- - 1)}{2} p \cong \frac{N_- N_+}{2} p = \frac{\dot{N}_{SB}}{2 f_R} \qquad (17)$$

Let $\dot{N}_{SB}^{Mea}$ the measured SB counting rate:

$$\dot{N}_{SB}^{Mea} = \dot{N}_{SB} - \dot{N}_{SB}^{Ac} = \dot{N}_{SB}(1 - R) = \dot{N}_{SB}\left(1 - \frac{\dot{N}_{SB}}{2 f_R}\right) \qquad (18)$$

From (18) the actual SB counting rate $\dot{N}_{SB}$ can be finally evaluated:

$$\dot{N}_{SB} = f_R\left(1 - \sqrt{1 - \frac{2\dot{N}_{SB}^{Mea}}{f_R}}\right) \cong \dot{N}_{SB}^{Mea}\left(1 + \frac{\dot{N}_{SB}^{Mea}}{2 f_R}\right) \qquad (19)$$

In the last term of (19) a second order approximation has been used (the error introduced is less than 10% if $\dot{N}_{SB}^{Mea} \le 0.36 f_R$ and less than 0.5% if $\dot{N}_{SB}^{Mea} \le 0.18 f_R$, in DAΦNE $f_R \cong 3\ MHz$). Expression (19) allows finally evaluating the systematic error due to accidentals counts in the single colliding bunch mode of operation:

$$\frac{\Delta\dot{N}_{SB}}{\dot{N}_{SB}} = \frac{\dot{N}_{SB} - \dot{N}_{SB}^{Mea}}{\dot{N}_{SB}} \cong \frac{\dot{N}_{SB}^{Mea}}{2 f_R + \dot{N}_{SB}^{Mea}} \qquad (20)$$

The result for the case of *n* colliding bunches, with the same number of particles per bunch (but different between the two beams), can be derived in the same way obtaining:

$$\frac{\Delta\dot{N}_{SB}}{\dot{N}_{SB}} = \frac{\dot{N}_{SB} - \dot{N}_{SB}^{Mea}}{\dot{N}_{SB}} \cong \frac{\dot{N}_{SB}^{Mea}}{2n f_R + \dot{N}_{SB}^{Mea}} \qquad (21)$$

In the previous analysis the bandwidth (BW) of the monitor electronics has been assumed not to be so large to discriminate events within the bunch itself but large enough to discriminate among adjacent bunches.

In DAΦNE where $f_R \cong 3\ MHz$ and the maximum number of bunches per ring is $h = 120$ this condition implies a bandwidth $f_{BW} \cong hf_R \cong 360\ MHz$. The quantity f_{BW} indicates the maximum rate measurable by the luminosity monitor and implies that if the time distance between two events is $< 1/f_{BW}$ then they will be counted by the system as a single event. As reported in section 3.3, the DAΦNE luminosity monitor BW is 18 MHz so that the related effects must be taken into account. Let now consider a collider with a total of *h* buckets filled every *m-th* (*m* will be indicated as *filling module*). The number of bunches n_B that fall inside the time window $1/f_{BW}$ is given by:

$$n_B = \mathrm{int}\left(\frac{hf_R}{mf_{BW}}\right) \tag{22}$$

In this situation the beam can be considered as composed by 'macrobunches' with $n_B N_+$ particles each. Redefining accidentals as double SB event inside the macrobunch then the probability of accidentals is given by:

$$\binom{n_B N_-}{2}\left(N_+ p\right)^2 \tag{23}$$

If the total number of bunches per ring is *n* then the accidental counting rate is:

$$\dot{N}_{SB}^{Ac} = \frac{n}{n_B}\binom{n_B N_-}{2}\left(N_+ p\right)^2 f_R = \frac{nN_-\left(n_B N_- - 1\right)}{2}\left(N_+ p\right)^2 f_R \cong \frac{nn_B}{2}\left(N_- N_+ p\right)^2 f_R \tag{24}$$

The SB counting rate is:

$$\dot{N}_{SB}^{Ac} = \frac{n}{n_B}\binom{n_B N_-}{2}\left(N_+ p\right)^2 f_R = \frac{nN_-\left(n_B N_- - 1\right)}{2}\left(N_+ p\right)^2 f_R \cong \frac{nn_B}{2}\left(N_- N_+ p\right)^2 f_R \tag{25}$$

Analogously to the larger bandwidth case, it can be obtained:

$$\dot{N}_{SB} = \frac{nf_R}{n_B}\left(1 - \sqrt{1 - \frac{2\dot{N}_{SB}^{Mea} n_B}{nf_R}}\right) \cong \dot{N}_{SB}^{Mea}\left(1 + \frac{\dot{N}_{SB}^{Mea} n_B}{2nf_R}\right) \tag{26}$$

and

$$\frac{\Delta\dot{N}_{SB}}{\dot{N}_{SB}} = \frac{\dot{N}_{SB} - \dot{N}_{SB}^{Mea}}{\dot{N}_{SB}} \cong \frac{\dot{N}_{SB}^{Mea}}{\frac{2nf_R}{n_B} + \dot{N}_{SB}^{Mea}} \cong \frac{\dot{N}_{SB}^{Mea} n_B}{2nf_R} \tag{27}$$

By using (22) one can write:

$$\frac{\Delta\dot{N}_{SB}}{\dot{N}_{SB}} \cong \frac{\dot{N}_{SB}^{Mea}}{2nf_R}\,\mathrm{int}\left(\frac{h}{m}\frac{f_R}{f_{BW}}\right) \cong \dot{N}_{SB}^{Mea}\frac{h}{m}\frac{1}{2nf_{BW}} \tag{28}$$

Expression (28) holds when $f_{BW} < h/m\ f_R$, otherwise expression (21) must be used. Moreover in deriving (26), (27) and (28) it has been neglected the contribution of accidentals with more than two SB events. The ratio between triple and double events is now in the BW limited case $n_B N_- N_+ p/3$. In order to make such a ratio a small number, the value of p must be properly set by regulating the threshold k_T. Table 1 shows, for DAΦNE, the minimum k_T values to be used for different m values in order to keep the ratio smaller than 0.1.

It is worth to remark that accidentals on GB events do not affect the background measurement when the SBBS method is used. In fact, the background acquisition, performed when the beams are separated out of collision, automatically includes GB accidentals. When the MBBS method is used, GB accidentals still do not affect the measurement as far as the current per bunch of the non-colliding bunches is the same of the colliding ones. When these currents are consistently different, a GB accidental contribution, properly scaled with the current per bunch of the colliding and non-colliding bunches, should be taken into account in the evaluation of the total error. Anyway in most of the existing colliders (DAΦNE included) even filling patterns of the bunches are used so that the GB accidental contribution can be neglected.

m	n_B	k_T
1	20	310
2	10	207
3	6	126
4	5	101

Table 1: Minimum energy threshold k_T to be used for different values of the filling module m. Case of DAΦNE with $f_{BW} = 18\ MHz$. The threshold values have been calculated in order to keep the ratio between triple and double SB events smaller than 0.1.

Finally ‘mixed’ accidentals due to contemporary detection of a SB event and of a GB one do not affect the error measurement. In fact in both SBBS and MBBS methods the background evaluation is performed in the situation where the only GB events are present, so that mixed accidentals do not exist at all. When the bunches are colliding a mixed accidental event is counted as a ‘good’ SB event and no contribution to the error is given. Actually a fraction of mixed accidentals can generate a systematic overestimate of the SB counts. In fact, some SB events with energy below the threshold k_T can receive from a simultaneous GB event the extra energy necessary for overcoming the threshold and for being counted as a ‘good’ event. Anyway in very good vacuum machines such as DAΦNE, the GB cross section is much smaller than the SB one and consequently mixed accidental counting rates are much smaller than the SB accidental ones. Moreover, as already said, only a fraction of the total number of mixed events will contribute to the error. These considerations allow assuming negligible the mixed accidental contribution.

Expression (20), (21) and (28) allow correcting the luminosity measurement from the systematic error due to accidentals. The accuracy of this correction will be now calculated. The only term in expressions (20), (21) and (28) that affects the accuracy is the one concerning $\dot{N}_{SB}^{Mea}$. If $\dot{N}_{SB}^{Mea}$ is the integration window duration, then $\dot{N}_{SB}^{Mea} = N_{SB}^{Mea} / t_w$ and, keeping in mind that $\sigma_{N_{SB}^{Mea}} = \sqrt{N_{SB}^{Mea}}$, it can be easily derived:

$$\frac{\sigma_{\dot{N}_{SB}^{Mea}}}{\dot{N}_{SB}^{Mea}} = \sqrt{\frac{1}{t_w}\frac{1}{\dot{N}_{SB}^{Mea}} + \frac{\sigma_{t_w}^2}{t_w^2}} \tag{29}$$

σ_w will indicate throughout the paper the standard deviation of a generic quantity *w*.

Another term affecting accuracy is generated by the second order approximation of the square root used in deriving the above-mentioned expressions. The complete error is finally given by:

$$\frac{\sigma_{\dot{N}_{SB}}}{\dot{N}_{SB}} = \sqrt{\left(\frac{\sigma_{\dot{N}_{SB}^{Mea}}}{\dot{N}_{SB}^{Mea}}\right)^2 + \left(\frac{\sigma_{\dot{N}_{SB}}}{\dot{N}_{SB}}\right)_{Approx.}^2} \tag{30}$$

In DAΦNE the CPU that controls the luminosity monitor performs a high level operation in 16 ms, so it is possible to assume $\sigma_{t_w} = 16/\sqrt{12}\ ms = 4.62\ ms$. Presently in a typical measurement $t_w = 3\ s$ and $\dot{N}_{SB}^{Mea} = 150\ kHz$. As already mentioned in this section, the approximation with such a counting rate gives an error smaller than 0.5 % (the revolution frequency is ~ 3 MHz). Using all this data in (29) and (30) it is possible to obtain:

$$\frac{\sigma_{\dot{N}_{SB}}}{\dot{N}_{SB}} = 5.4 \times 10^{-3} \tag{31}$$

4.1.2 Energy threshold calibration

Let us now analyze the systematic error that can affect the GB calibration procedure. First of all, in acquiring a GB spectrum, single stored beam and small counting rate must be preferred in order to avoid contaminations due to the other beam (collision and induced shower products) and to accidentals. In DAΦNE the calibration is typically performed with small stored current (~10 mA) in multibunch fills (~ 10 bunches). In this way the obtained counting rate is around 10 kHz and both the contamination percentages due to accidentals and cosmic rays (counting rate < 1 Hz) are of the order of 10^{-4}. Additionally a minimum number of samples must be collected for minimizing statistical fluctuations. It is reasonable to keep such error below the one of expression (5), which is ~ 0.01. To fulfill this requirement at least 10 ksamples per (ADC) channel are necessary. In DAΦNE, where usually 256 channels are used, a good spectrum should contain about 2.5 Msamples.

The linearity of the ADC chain is very good, see Figure 5. The standard deviation of a sampled value is about 2 channels when a total of 256 channels is used. The channel width, in the case of DAΦNE is typically 2.5 MeV, so that the standard deviation in terms of energy, or in other words the energy resolution of the ADC chain, is 5 MeV.

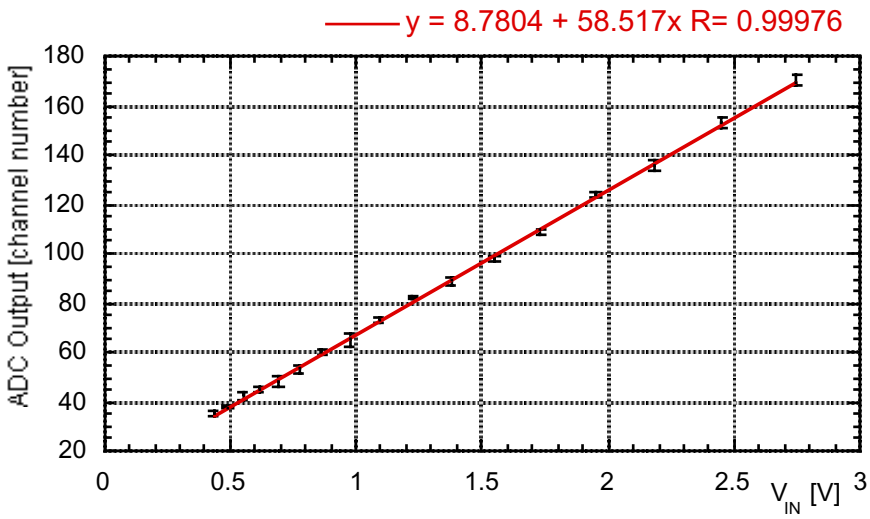

Figure 5: Photon energy analysis system linearity measurement.

The error propagation of expression (6) is:

$$\frac{\sigma_{k_T}^2}{k_T^2} = \frac{\sigma_{k_{\max}}^2}{k_{\max}^2} + \frac{\left(x_{\max} - x_T\right)^2}{\left(x_{\max} - x_0\right)^2\left(x_T - x_0\right)^2}\sigma_{x_0}^2 + \frac{\sigma_{x_T}^2}{\left(x_T - x_0\right)^2} + \frac{\sigma_{x_{\max}}^2}{\left(x_{\max} - x_0\right)^2} \tag{32}$$

It is worth to point out that the higher x_T, the smaller the error.

The quantity $k_{\max}$ is evaluated by expression (2) and the dominant error is due to the ω measurement, which can have a standard deviation of 0.8 MeV, if evaluated by using the machine parameters:

$$\frac{\sigma_{k_{\max}}}{k_{\max}} = 8 \cdot 10^{-4} \tag{33}$$

The quantity x_0 and its standard deviation σ_{x_0} can be evaluated by the linearity measurement of Figure 5. In fact the value of the linear fit $x = mV + x_0$, for zero input signal is just the x_0 value. If a least square fit is used:

$$x_0 = \frac{\left(\sum_{n=1}^{N} V_n^2\right)\left(\sum_{n=1}^{N} x_n\right) - \left(\sum_{n=1}^{N} V_n\right)\left(\sum_{n=1}^{N} V_n x_n\right)}{N\left(\sum_{n=1}^{N} V_n^2\right) - \left(\sum_{n=1}^{N} V_n\right)^2} \tag{34}$$

and

$$\sigma_{x_0}^2 = \frac{1}{N - \left(\sum_{n=1}^{N} V_n\right)^2 \Big/ \sum_{n=1}^{N} V_n^2}\sigma_x^2 \tag{35}$$

where the same standard deviation σ_x has been assumed for all the N measured points, which is, in DAΦNE, a realistic assumption when at least 1 ksample per point is taken.

It was previously mentioned that, in the case of the DAΦNE monitor, the standard deviation σ_x of a sampled value is:

$$\sigma_x = 2 \; channels \tag{36}$$

Using the results of several linearity tests in the expression (35), it is possible to obtain for DAΦNE:

$$\sigma_{x_0} = 1.2\sigma_x = 2.4 \; channels \tag{37}$$

The quantity x_T is measured on the experimental GB spectrum, thus it is reasonable to assume that:

$$\sigma_{x_T} = \sigma_x = 2 \; channels \tag{38}$$

The evaluation of the quantity $x_{\max}$ passes through expression (5) for the calculation of $y_{\max}$. If the statistical fluctuation on the flat area of the GB spectrum is contained within 0.01 (at least 10 ksample per channel), than making the convolution with the error of expression (5):

$$\sigma_{y_{\max}} / y_{\max} = 0.0164 \tag{39}$$

The dependence of $\sigma_{x_{\max}} / x_{\max}$ from $\sigma_{y_{\max}} / y_{\max}$ is given by:

$$\frac{\sigma_{x_{\max}}}{x_{\max}} = \left| \frac{\partial y\left(x = x_{\max}\right)}{\partial x} \; \frac{x_{\max}}{y_{\max}} \right|^{-1} \frac{\sigma_{y_{\max}}}{y_{\max}} \tag{40}$$

where the argument of the absolute value operator can be calculated using the theoretical GB cross section convoluted with the resolution function of the calorimeter (see section 2.2 and Appendix B). A numerical evaluation of expression (40), for the case of DAΦNE, has been performed obtaining the fitting function:

$$\frac{\sigma_{x_{\max}}}{x_{\max}} = \left| -2.051 \cdot 10^{-3} \left(\frac{\sigma_E}{E} \right)^2_{\max} + 1.249 \left(\frac{\sigma_E}{E} \right)_{\max} - 7.866 \cdot 10^{-1} \right| \frac{\sigma_{y_{\max}}}{y_{\max}} \tag{41}$$

where $\left(\sigma_E / E\right)_{\max}$ is the calorimeter resolution at the energy $k_{\max}$ (see expression (14)). The error introduced by using this fitting function is at least one order of magnitude smaller than the value of (39) in the range of resolution from 0.01 to 0.15. Using the DAΦNE energy of 0.51 GeV in (14) and the consequent result in (39), $\sigma_{x_{\max}} = 0.00116 \; x_{\max}$ is obtained. Actually this error must be convoluted with the standard deviation $\sigma_x = 2$ of a sampled value, see expression (36). As in DAΦNE $x_{\max}$ is typically 170 200, the σ_x contribution is dominant and it can be assumed:

$$\sigma_{x_{\max}} = \sigma_x = 2 \;\; channels \tag{42}$$

This is an important result indicating that the contribution of the calorimeter resolution to the error is much smaller than the one due the ADC system resolution.

At this point we have all the elements necessary to evaluate, in the case of DAΦNE, the contribution to the error that expression (32) gives. In a typical calibration with 256 channels $x_0 = 6$, $x_{\max} = 185$ and $x_T = 75$. Thus:

$$\frac{\sigma_{k_T}^2}{k_T^2} = 6.40 \cdot 10^{-7} + 7.93 \cdot 10^{-5}\,\sigma_{x_0}^2 + 2.10 \cdot 10^{-4}\,\sigma_{x_T}^2 + 3.12 \cdot 10^{-5}\,\sigma_{x_{\max}}^2 \tag{43}$$

and using (37), (38) and (42):

$$\frac{\sigma_{k_T}}{k_T} = 3.8\ \% \tag{44}$$

The last step consists in deriving the error contribution that (44) gives during the SB cross-section evaluation:

$$\frac{\sigma_{\zeta_{SB}}}{\zeta_{SB}(k_T)} = \left| \frac{\partial \zeta_{SB}(k = k_T)}{\partial k} \frac{k_T}{\zeta_{SB}(k_T)} \right| \frac{\sigma_{k_T}}{k_T} \tag{45}$$

the quantities necessary for the evaluation of the absolute value operator argument can be found in Appendix A. For convenience, such term versus k_T has been calculated and the results are showed in Figure 6. In the previous example, to $x_T = 75$ corresponds, using expression (6), $k_T = 197\,MeV$. Thus the error contribution, due to the calibration, on the SB cross-section is:

$$\frac{\sigma_{\zeta_{SB}}}{\zeta_{SB}(k_T)} = 1.21\,\frac{\sigma_{k_T}}{k_T} = 4.6\ \% \tag{46}$$

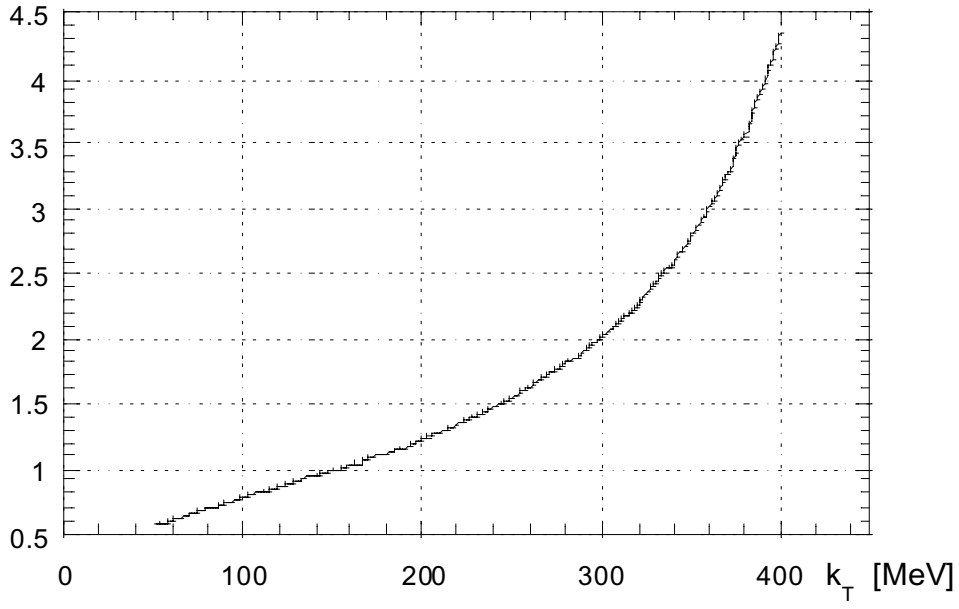

Figure 6: Single bremsstrahlung error factor vs. energy threshold. Analytical Result.

4.1.3 Angular Acceptance of the collimator-calorimeter system

As already mentioned in section 3.1, the solid angle portion accepted by the calorimeter, when the 2 cm diameter collimator is inserted, is included in the acceptance cone (AC) with vertex at IP and axis aligned on the 12.5 mrad horizontal crossing angle of the DAΦNE IR. The distance between the IP and the calorimeter is 6 m, so that the semi-aperture angle α_{AC} of the acceptance cone is 1.667 mrad. By integrating the SB cross-section over this solid angle it can be obtained that a percentage of ~ 70% of the emitted SB photons are accepted by the collimator-calorimeter system. In this section it will be investigated the effect of different cut-off energies k_T and also the case where the SB photon distribution is not centered on the collimator, situation that can happen when the tangent to the beam trajectory at IP does not coincide with the axis of the AC. Finally the effects of the beam dimension at IP will be also considered.

In the case of DAΦNE, by integrating the SB cross-section (see Appendix A) within the acceptance cone for different values of k_T, it is possible to obtain the plot of Figure 7. The linear fitting function allows evaluating the percentage of accepted photons P_{AC} for a given cutoff energy k_T, with accuracy always better than 10^{-3}:

$$P_{AC}(k_T) = \frac{\zeta_{SB}(\alpha_{AC} = 1.667\,mrad, k_T)}{\zeta_{SB}(\alpha_{AC} = \pi/2, k_T)} = 7.7801 \cdot 10^{-5} k_{T(MeV)} + 0.69779 \qquad (47)$$

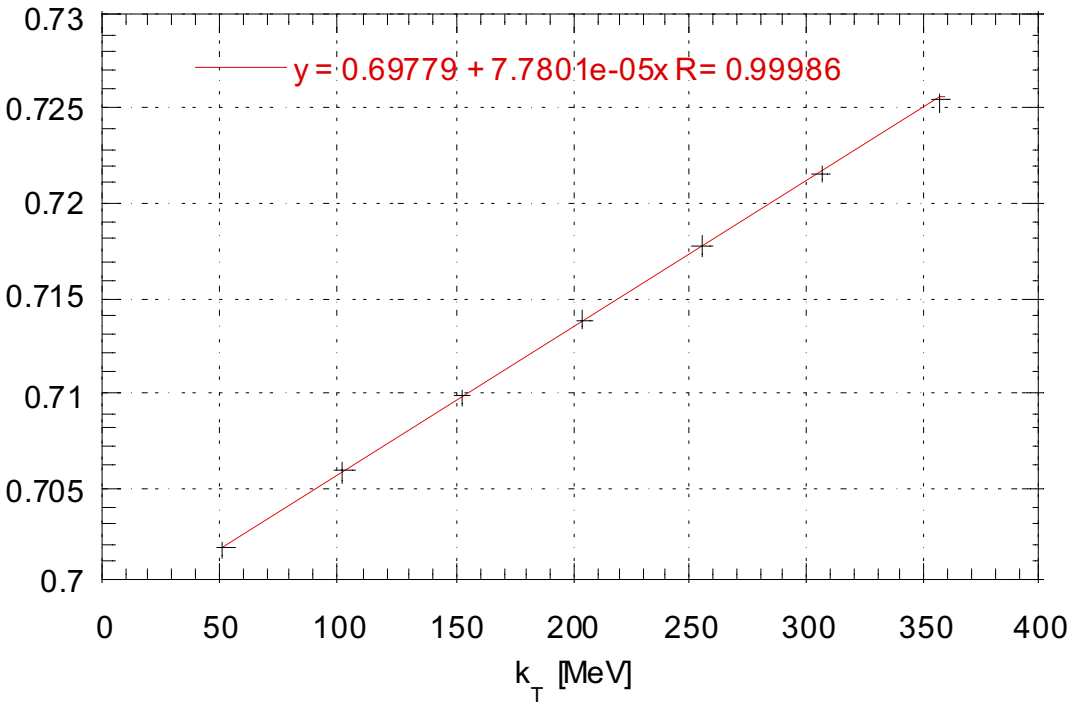

Figure 7: Percentage of accepted single bremsstrahlung photons vs. energy threshold. Analytical result. Case of a circular collimator of 1 cm radius placed in front of the calorimeter 6 m far from the IP and with symmetry axis coincident with the tangent to the beam trajectory at the IP.

The previous expression has been derived in the case where the two axes of the AC and of the SB distribution coincide preserving the cylindrical symmetry. In the case that the IP transverse position and/or the tangent to the beam trajectories at IP do not have the design values, then the cylindrical symmetry is broken and an analytical expression for the SB cross-section cannot be obtained. In order to evaluate the systematic error generated in this situation a Monte Carlo routine has been developed. The photon energy k and the emission angle a, are extracted according to the differential cross-section $\partial^2\zeta_{SB}/\partial k\,\partial\alpha$ while a second angle φ is uniformly extracted (in the plane perpendicular to the AC axis) between 0 and 2π in order to fulfill the cylindrical symmetry, see Figure 8. The photons are then propagated up to the collimator, which now can have arbitrary position and shape. Figure 9 and 10 show the results obtained, with $5\cdot10^5$ extracted photons, in the case of DAΦNE with the circular 2 cm diameter collimator 6 m far from the IP.

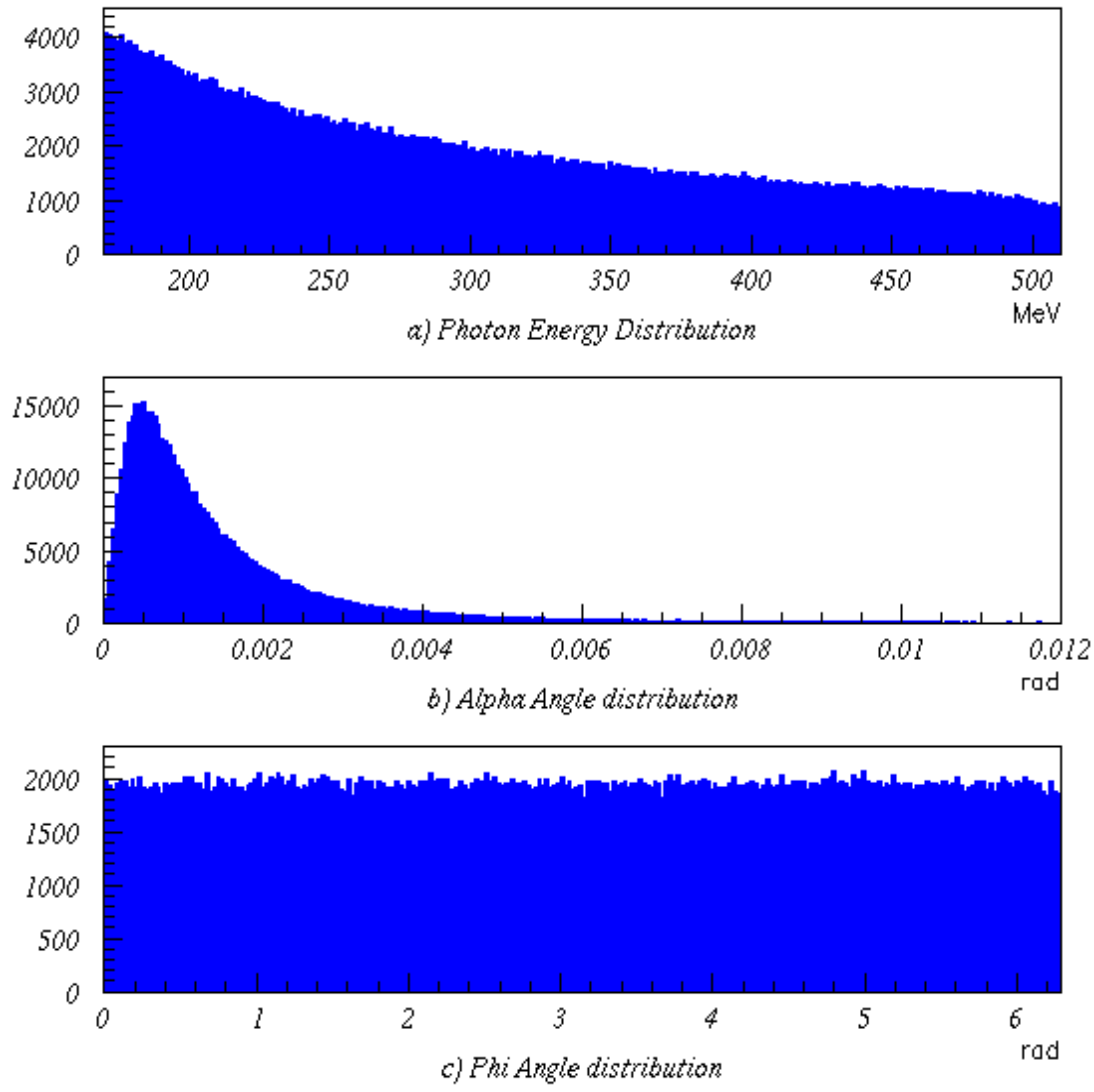

Figure 8: SB Monte Carlo routine, $5\cdot10^5$ extracted photons: a) photon energy k histogram in MeV (extraction starts @ 170 MeV), b) α angle histogram in rad and c) φ angle histogram in rad.

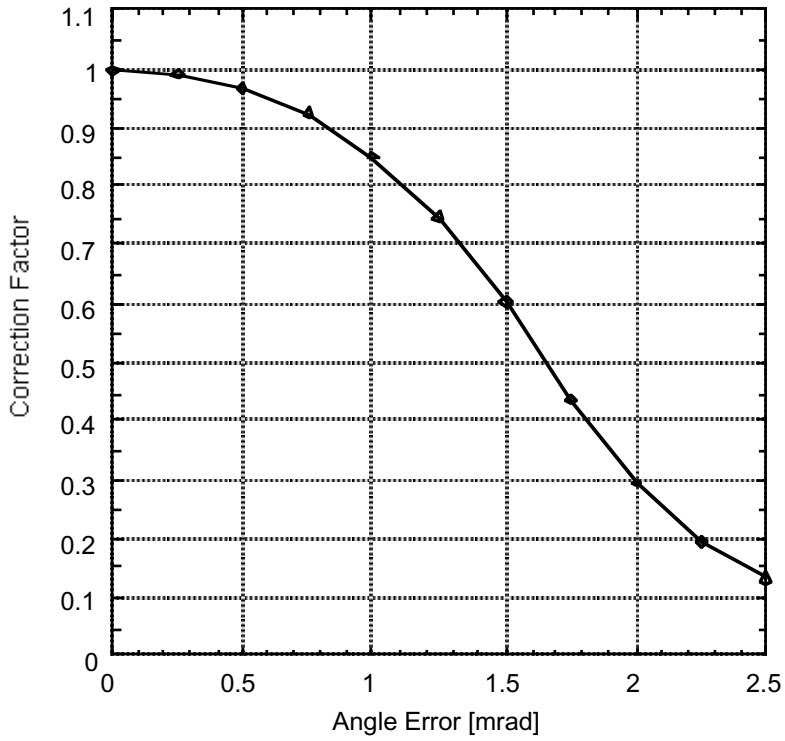

Figure 9: Correction factor for expression (47) vs. the angle between the acceptance cone axis and the tangent to the beam trajectory at IP. Monte Carlo result.

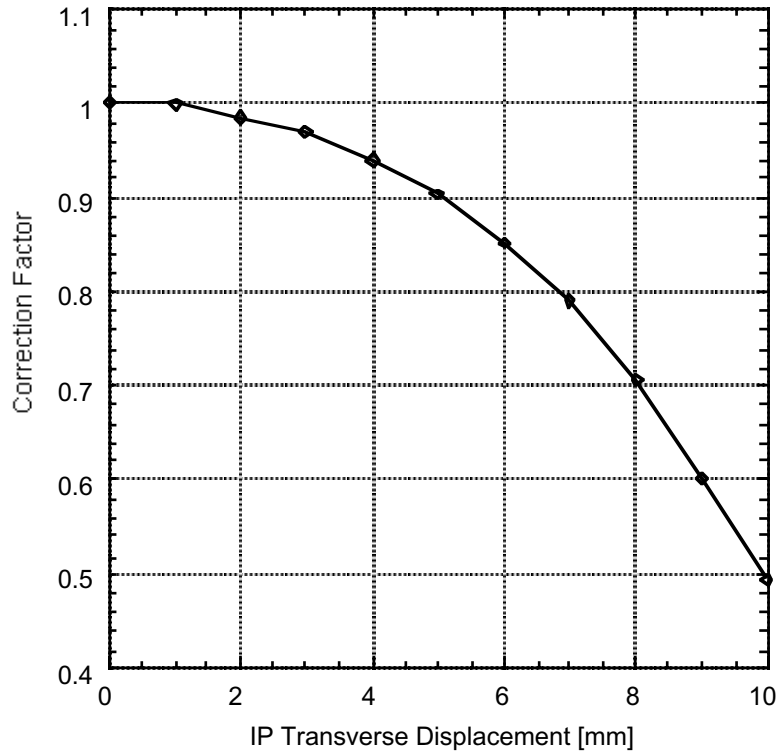

Figure 10: Correction factor for expression (47) vs. IP displacement. Monte Carlo result.

In Figure 9, the factor to be used for correcting the value obtained by expression (47) is shown as a function of the angle existing between the AC axis and the tangent to the beam trajectory at IP. This factor practically does not depend on k_T. Figure 10 shows instead the correcting factor to be used when a transverse displacement of IP exists. Also this factor does not depend on k_T. In DAΦNE the vertical and horizontal crossing angles and the IP transverse position can be measured with a standard deviation of 0.5 mrad and 0.5 mm respectively. From Figures 9 and 10 it can be seen that with this values the contribution to the systematic error is negligible for the displacement and – 3.2 % for the angle. Thus it is possible to write:

$$\frac{\sigma_{P_{AC}}}{P_{AC}} = -3.2\ \% \tag{48}$$

So far the IP has been treated as a point-like source, now the effects due to the beam finite size will be investigated. With the DAΦNE present operating configuration the r.m.s. sizes and divergences at IP are:

$$\begin{aligned} \sigma_x &= 2.2\ mm \quad \sigma'_x = 0.38\ mrad \\ \sigma_y &= 15.0\ \mu m \quad \sigma'_y = 0.27\ mrad \end{aligned} \tag{49}$$

A crude but conservative way to estimate the beam size effects consists in taking the larger values in (49) and treating them as pure indeterminacies in position and angle. In this way, by convoluting the 2.2 mm with the above-mentioned 0.5 mm measurement error and the 0.38 mrad with the 0.5 mrad measurement error, total indeterminacies of 2.26 mm and 0.63 mrad are obtained. By using these values in Figure 9 and 10 the contributions to the systematic become –5.4 % for the angle and of –1.9 % for the displacement. By putting together these two terms, it is finally obtained:

$$\left.\frac{\sigma_{P_{AC}}}{P_{AC}}\right|_{COR.} = -5.7\ \% \tag{50}$$

In this section the uncertainty on the collimator-calorimeter system position was not considered. In fact, those parts, which are located 6 m far from the IP, are placed with a precision of 0.5 mm and the contribution given to the angular acceptance error is negligible.

4.1.4 Aluminum thin window electromagnetic showers

In section 3.1 it has been mentioned that GB and SB photons, before arriving to the proportional counter, must pass through an aluminum window 1.5 mm thick. Of course electromagnetic showers will be occasionally generated on the metallic window and the pairs created in the process will produce a signal on the anticoincidence scintillator placed in front of the calorimeter. The result will be that the counts due the shower generating photons will be neglected. In the case of showers induced by GB photons, no systematic error is introduced because, in both the SBBS and MBBS techniques, the measured background will also include these shower effects. On the contrary, when the generating photons are due to SB, a systematic underestimate of the luminosity will result. Let us now evaluate this effect.

The number of atoms per unit volume in the window material N_A, is given by:

$$N_A = \frac{\rho}{A m_p} \tag{51}$$

where ρ is the material density, A the atomic weight and m_p the proton mass. Let now ζ be the photon cross-section in the window material (in the energy range of interest ζ is strongly dominated by pair formation term), and t the thickness of the window. Thus the probability that a photon passing through the window generates a shower is given by:

$$P_S = \zeta N_A t = \frac{\zeta \rho}{A m_p} t \tag{52}$$

In the case of DAΦNE $\rho = 2.70\ g/cm^3$, $A = 27$, $t = 0.15\ cm$ and $\zeta = 1.22 \pm 0.09\ barn/atom$ in the energy range $100 \div 510\ MeV$ [15], so the systematic error due the window showers is:

$$\frac{\Delta \dot{N}_{SB}}{\dot{N}_{SB}} = -P_S = -1.09 \pm 0.08\ \% \tag{53}$$

The contribution, evaluated by (52), of shower events on the polystyrene scintillator is negligible.

4.1.4 Various.

Other effects that can generate systematic errors on the luminosity measurement are undesired counts due to DB photons, to cosmic rays and to bhabha particles.

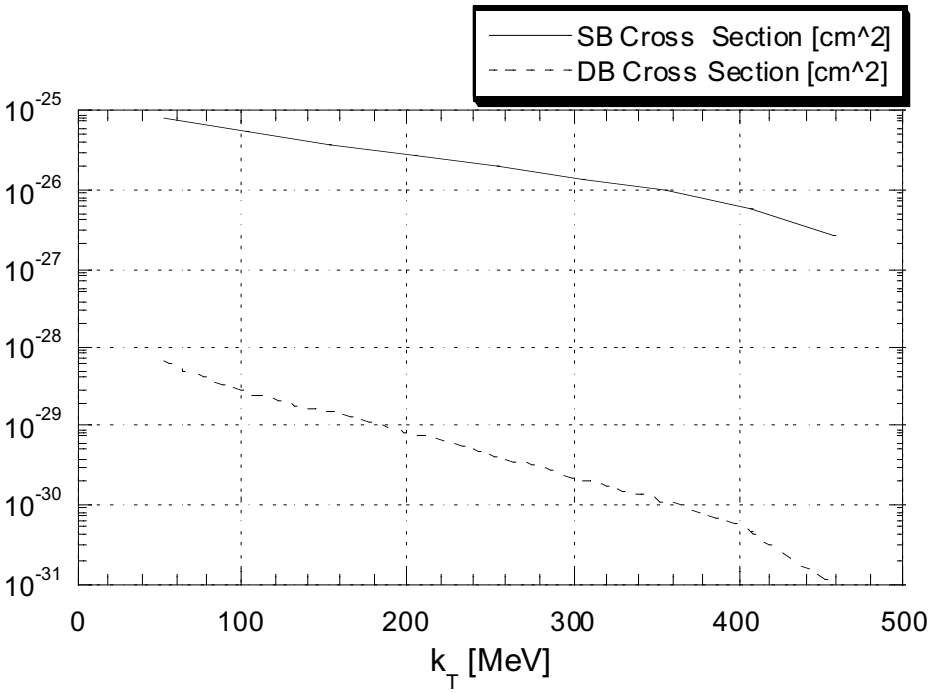

Figure 11: Single and double bremsstrahlung cross sections vs. energy threshold. Analytical Result.

Figure 11 allows a comparison between the SB and DB cross-sections as a function of the energy threshold k_T.Because DB cross-section is at least 3 orders of magnitude smaller than the SB one, for all the reasonable k_T values, than DB contribution is always negligible.

Measured counting rates due to cosmic rays, when no beam is stored, have values of the order of the Hz. Counting rates during luminosity and background measurements are never smaller than 10 kHz, thus the cosmic ray contribution can be neglected as well.

As far as bhabha events are concerned, the combined action of the clearing field of the splitter magnet and of the scintillator anti-coincidence does not allow any charged particle to generate undesired counts during the measurement.

Finally, k_T calibration checks performed at distance of several days each other demonstrated the very good stability of the system and of all its parts (PMT gain, electronics, …).

4.2. Statistical errors

The statistical error is due to the fluctuations in the counting rate measurements. The two different cases of MBBS and SBBS must be separately analyzed.

4.2.1 Statistical error with the SBBS technique

In the SBBS technique the SB counting rate is obtained by the simple operation:

$$\dot{N}_{SB} = \dot{N}_T - \dot{N}_{BK} \tag{54}$$

where $\dot{N}_T$ and $\dot{N}_{BK}$ indicate the counting rates measured with the beams in and out of collision respectively. Keeping in mind that $\dot{N}_Y = N_Y / t_w$ and that $\sigma_{N_Y} = \sqrt{N_Y}$ ($Y = T$ or BK and t_w is the integration window duration), it can be derived:

$$\frac{\sigma^2_{\dot{N}_{SB}}}{\dot{N}^2_{SB}} = \frac{1}{t_w}\frac{\dot{N}_T + \dot{N}_{BK}}{\left(\dot{N}_T - \dot{N}_{BK}\right)^2} + \frac{\dot{N}_T^2 + \dot{N}_{BK}^2}{\left(\dot{N}_T - \dot{N}_{BK}\right)^2}\frac{\sigma^2_{t_w}}{t_w^2} \tag{55}$$

that, if $\dot{N}_T >> \dot{N}_{BK}$, becomes:

$$\frac{\sigma^2_{\dot{N}_{SB}}}{\dot{N}^2_{SB}} \approx \frac{1}{t_w}\frac{1}{\dot{N}_T} + \frac{\sigma^2_{t_w}}{t_w^2} \tag{56}$$

From (55) and (56) it is possible to see that the contribution of this error can be controlled by properly setting the duration of the integration window t_w. In the case of DAΦNE $\dot{N}_T$ is typically kept (by properly setting the discriminator threshold) around 150 kHz and $\dot{N}_{BK}$ is around 10 kHz. As already specified in section 4.1.1 $\sigma_{t_w} = 4.62\ ms$ and using an integration window $t_w = 3\ s$:

$$\frac{\sigma_{\dot{N}_{SB}}}{\dot{N}_{SB}} = 2.3 \times 10^{-3} \tag{57}$$

where the contributions of the terms in expression (55) are balanced. For larger time windows the total error decreases and the contribution of the σ_{t_w} term becomes smaller and vice versa.

4.2.2 Statistical error with the MBBS technique

In the case of the MBBS technique the SB counting rate is obtained by expression (13). The standard deviation of this expression is:

$$\sigma^2_{\dot{N}_{SB}} = \frac{1}{t_w}\left[\dot{N}_C + \dot{N}_{NC}\left(\frac{I^+_C}{I^+_{NC}}\right)^2\right] + \left[\dot{N}^2_C + \dot{N}^2_{NC}\left(\frac{I^+_C}{I^+_{NC}}\right)^2\right]\frac{\sigma^2_{t_w}}{t^2_w} + \left(\dot{N}_{NC}\frac{I^+_C}{I^+_{NC}}\right)^2\left[\left(\frac{\sigma_{I^+_C}}{I^+_C}\right)^2 + \left(\frac{\sigma_{I^+_{NC}}}{I^+_{NC}}\right)^2\right] \tag{58}$$

where $\dot{N}_C$ and $\dot{N}_{NC}$ are the counting rates relative to the colliding and non colliding bunches respectively and I^+_C and I^+_{NC} are the total currents of the colliding and non colliding positron bunches. If n_C and n_{NC} are the numbers of colliding and non-colliding bunches respectively and assuming even filled buckets, so that $I^+_Y = n_Y I_B$ and $\sigma^2_{I^+_Y} = n_Y \sigma^2_{I_B}$ (where $Y = C, NC$ and I_B is the single bunch current), than expression (58) can be rewritten as:

$$\sigma^2_{\dot{N}_{SB}} = \frac{1}{t_w}\left[\dot{N}_C + \dot{N}_{NC}\left(\frac{n_C}{n_{NC}}\right)^2\right] + \left[\dot{N}^2_C + \dot{N}^2_{NC}\left(\frac{n_C}{n_{NC}}\right)^2\right]\frac{\sigma^2_{t_w}}{t^2_w} + \left(\dot{N}_{NC}\frac{n_C}{n_{NC}}\right)^2\left(\frac{1}{n_C} + \frac{1}{n_{NC}}\right)\left(\frac{\sigma_{I_B}}{I_B}\right)^2 \tag{59}$$

From expression (58) and (59) it can be seen that, this time, the window t_w controls only two terms of the error, the third term depends instead on the current measurement accuracy. Presently in DAΦNE the bunch-by-bunch current monitor allows measurements with 10% error. As a typical example, let $n_C = 50$, $n_{NC} = 5$, $\dot{N}_C = 150\ kHz$, $\dot{N}_{NC} = 1\ kHz$, $t_w = 3\ s$ and $\sigma_{t_w} = 4.62\ ms$ then:

$$\frac{\sigma_{\dot{N}_{SB}}}{\dot{N}_{SB}} = 4.2 \times 10^{-3} \tag{60}$$

In this particular case, the contribution of the current term in (59) is almost twice the one of the other two terms.

4.3 Total error

As far as the statistical error is concerned, it has been shown in the previous section that it can be easily kept down to few parts per thousand. It is worth to remark that when a relative luminosity measurement is needed and the stability of the monitor is good, the only error affecting the measurement is the statistical one. The small values of expressions (57) and (60) indicate that very precise measurements can be already obtained with an integration window of only 3 seconds. This means a precise measured value every three seconds, feature that practically allows a real time optimization of any machine parameter versus luminosity.

In section 5.3 some examples of the extensive use done in DAΦNE of such measurement technique will be showed. Summarizing, for a typical relative luminosity measurement the statistical error is:

$$\left.\frac{\sigma_L}{L}\right|_{Statistical} = \begin{cases} 0.23\,\% & \textit{with SBBS} \\ 0.42\,\% & \textit{with MBBS} \end{cases} \qquad (61)$$

Concerning the systematic error affecting the absolute luminosity measurements, it has been already shown that it does not depend on the background subtraction scheme used. The measured luminosity values must be first corrected from the effects due to accidentals, angular acceptance and thin window showers using expressions (28), (47) and (53) respectively. The accuracy of these correction factors are given for DAΦNE by expressions (31), (50) and (53). The angular acceptance indeterminacy (50), –5.7 %, completely dominates the other two that are always smaller than 0.1%. The other important term is the one concerning the threshold calibration that according to (46) generates a contribution of 4.6 %. The convolution between these two major terms finally gives the typical systematic error on a luminosity absolute value measurement:

$$\left.\frac{\sigma_L}{L}\right|_{Systematic} = \begin{matrix} +4.6\,\% \\ -7.3\,\% \end{matrix} \qquad (62)$$

Expression (62) presents different standard deviations between the plus and minus cases because, in the DAΦNE monitor setup, the indeterminacy on the angular acceptance always leads to a measurement underestimate (see Figures 9 and 10).

As already said in sections 2.2 and 2.3, special attention must be paid in avoiding spurious counts due to shower products induced by beam lost particles. The use done of shields, clearing fields and charged particle anticoincidences allows to reduce the effect and to push the $\dot{N}_{dI}$ term in expression (7) down to negligible values. Anyway it can happen that for some particular machine and IR configurations the above-mentioned cures are not sufficient and that a non-negligible number of shower-induced photons are able to reach the calorimeter front face generating spurious counts. It is very important to detect when such a situation happens. In DAΦNE for this task, it is exploited the fact that the beam lifetime is dominated by Touschek effect. So by changing the beam transverse dimension (using a skew quadrupole for example) it is possible to modify the beam density and thus the beam lifetime. This operation is performed when the beams are out of collision, or better, when a single beam is stored (the one pointing the calorimeter) and the related calorimeter counting rates are recorded. If the rates depend on the beam lifetime, then the $\dot{N}_{dI}$ term is not negligible and spurious counts will affect the luminosity measurements. In such a case it is necessary to modify the machine configuration (orbits at IR, scrapers, …) for eliminating the problem.

5. Experimental Results.

5 .1. Experimental GB Spectra

Figure 12 shows an example of an experimental GB energy spectrum in DAΦNE. In the top part of the figure, a 256 channels (bins), 4.2 Msample spectrum is showed (solid line)

together with the theoretical differential cross-section (dashed line) (see Appendix B). The agreement between the two curves is quite good and the difference at the threshold channel position (channel 23) is due to the fact that in the theoretical function an ideal acquisition electronics has been assumed, while in the real case the resolution of the analog channel generates the finite value slope of the actual spectrum around the threshold position. In the bottom part of Figure 12, the GB modified spectrum, see section 2.2, is showed.

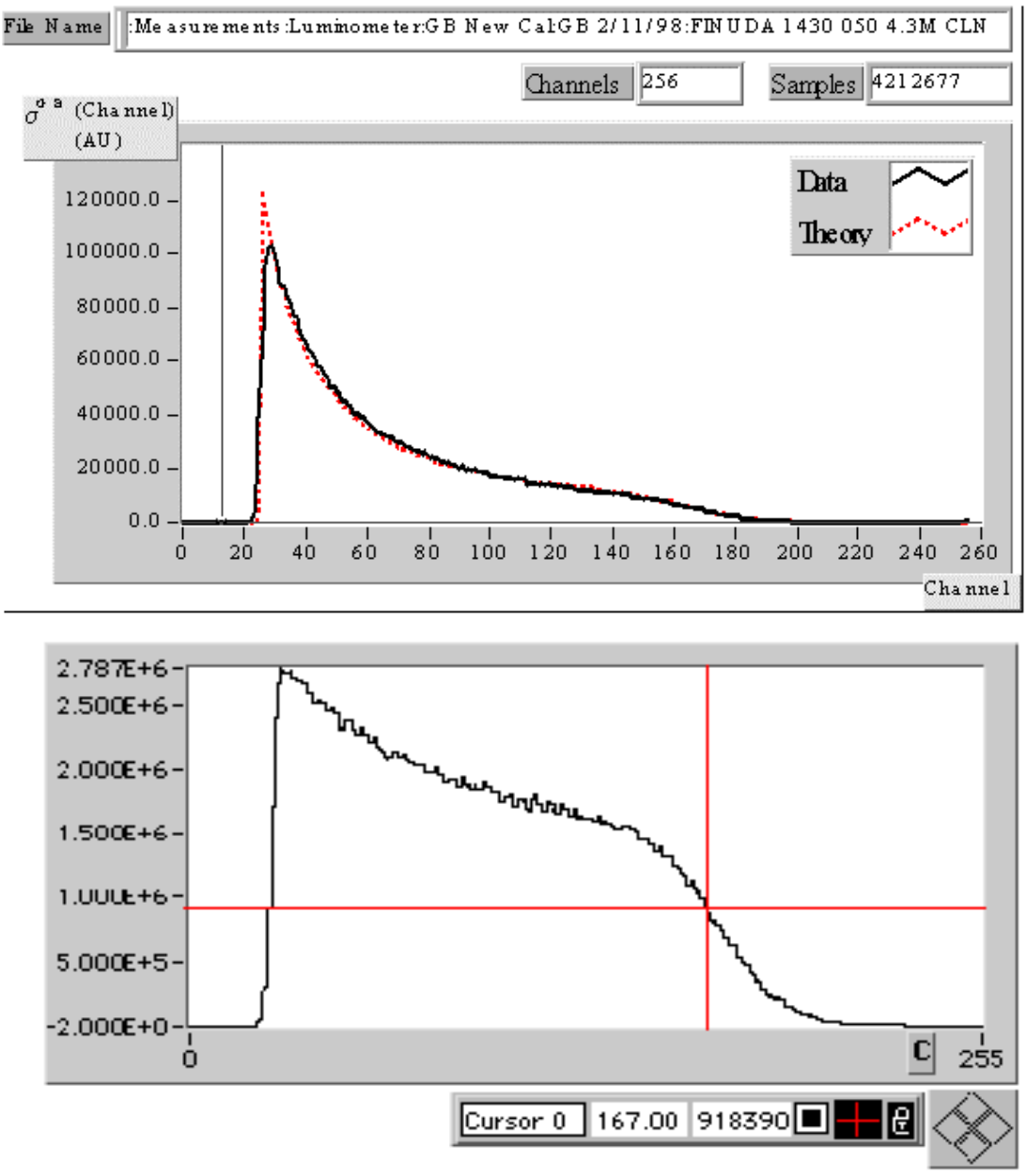

Figure 12: Top: gas bremsstrahlung experimental and theoretical spectra. Bottom: experimental gas bremsstrahlung modified spectrum.

5 .2. Absolute Luminosity Measurements

Figure 4 shows the luminosity monitor main window during an absolute value measurement using the SBBS method. The track inside the window indicates the calorimeter counting rate history, the horizontal scale is in seconds while the vertical one is in Hz. In this particular measurement, an integration time window of 20 s was selected so that each point in the plot shows the average counting rate over 20 s of data acquisition. The counting rate started from about 150 kHz and progressively decreased down to about 58 kHz at the moment the picture was taken. In this condition, the measurement is very stable with negligible statistical fluctuations. The background subtraction, by separating the beams and sampling the background (using the phase jump technique described in section 2.3), was performed at the beginning of the measurement, around the 20^{th} second, and at the end of the track, around the 2900^{th} second where a 'notch' is present. An energy threshold k_T of 170 MeV was used. The monitor window shows also a number of additional information related to the luminosity measurement: number of colliding bunches, beam currents, lifetimes and others.

As already said, at the present time two independent monitors are located in the KLOE IR, one facing the positron beam and the other the electron one. Simultaneous absolute measurements performed with the two monitors agree within the experimental error with differences usually smaller than 5 %.

The MBBS technique is not very used in DAΦNE. In fact during the tune-up of the luminosity, usually performed with single colliding bunches, the contribution to the final error due to the bunch by bunch current measurement system is strong (see expression (59) evaluated for the single colliding bunch case) and the SBBS method is preferred for accuracy and simplicity. On the other hand during the experiment data taking, the KLOE detector performs by itself the absolute luminosity measurement, while the DAΦNE monitor is used in the relative mode for keeping the luminosity optimized to the maximum. Anyway, dedicated tests for comparing the MBBS and the SBBS methods were performed and the results obtained agreed within the experimental error with differences always smaller than 10%.

As far as concerns the comparison between KLOE and DAΦNE absolute luminosity measurements, Figure 13 shows an example where several hours of measurements are compared. The data from 16:00 (4 p.m.) to 19:00 (7 p.m.) concern single bunch collisions during the luminosity tune-up: different machine parameters are changed for optimizing luminosity with the DAΦNE monitor performing fast measurements (one every 3 s). In this situation the KLOE luminosity measurement, which uses large angle bhabhas, does not collect enough statistics and suffers of consistent statistical fluctuations. Around 19:30 (7:30 p.m.) multibunches collisions begin and now, with the increased luminosity, the agreement between the two measurements becomes quite good.

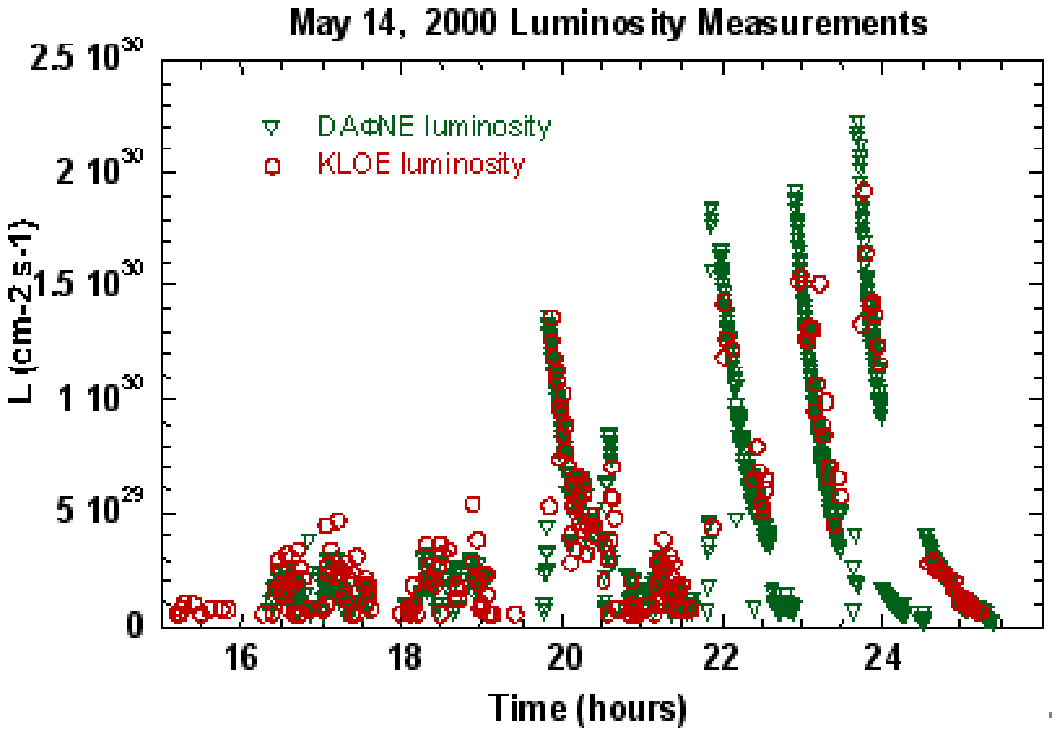

Figure 13:.Absolute luminosity measurements: a comparison with the KLOE experiment data.

5 .3. Relative Luminosity Measurements

Relative luminosity measurements play a fundamental role during the tuning of the IR for luminosity optimization. Every machine parameter that affects luminosity can be varied and the related luminosity can be simultaneously recorded. Because of the fast measurement capabilities of the luminosity monitor such scans can be systematically and extensively used for finding out the optimum value of parameters such as, among the others, vertical and horizontal overlap of the beams at IP, vertical and horizontal crossing angle at IP and longitudinal IP position. If such scan technique is used with very low current per bunch, the beam-beam effects become negligible and cross related measurements allow collecting important information concerning machine parameters such as optical functions at IP, crossing angles, emittance ratio and others. A more detailed description of these measurement techniques is reported in reference [3]. Figure 14 shows an example of scan of the mutual vertical position between the colliding beams versus luminosity. In this particular case, where the monitor pointing the positron beam was used, the positrons were kept fixed while a vertical bump localized at IR was applied to the electrons. The bump step was 5 μm and for each position 5 luminosity values were recorded. In the graph of Figure 14 the horizontal scale indicates in μm the vertical position of the electron beam while the vertical scale shows the luminosity values normalized with respect to the product of the beam currents, in order to remove the dependence of the measurement on the beam lifetimes. For each step, the couple of small squares indicates the 2 standard deviation segment centered on the average value of the

measured luminosity. The solid line is the gaussian fit of the measured data. A complete scan like that takes about 3.5 minutes to be completed.

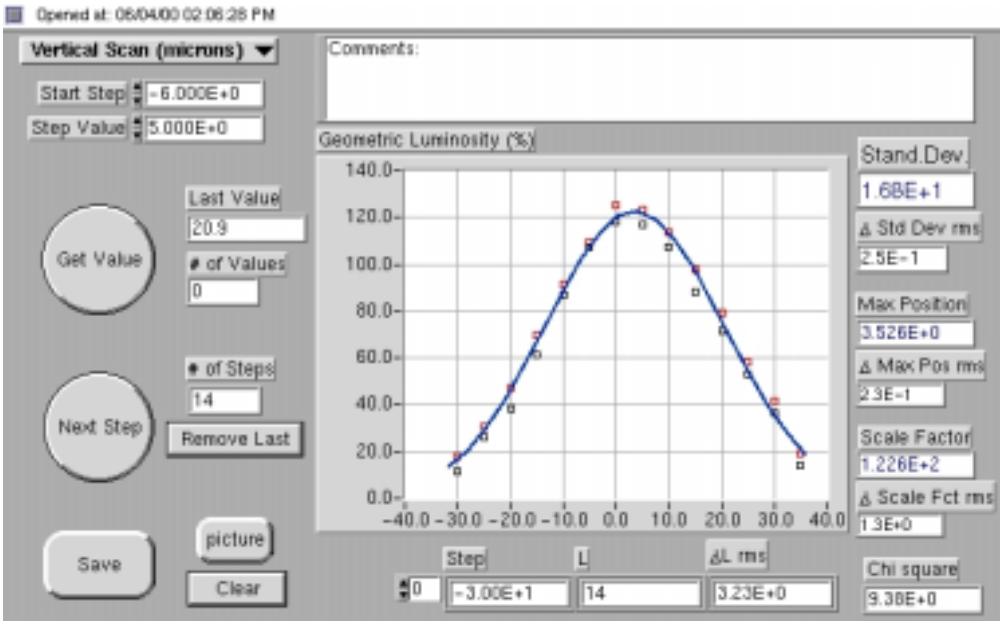

Figure 14:.An example of relative luminosity measurement: normalized luminosity vs. colliding beams mutual vertical position.

6. Conclusions.

The DAΦNE single bremsstrahlung luminosity monitor played and still plays a fundamental role in the machine tune-up during the luminosity performance optimization. In the relative mode it is able to delivery non-calibrated measurements every 3 seconds with accuracy, according to (61), of few parts per thousands. This capability allows real time optimization of whatever machine parameter versus luminosity and makes the implementation of an eventual luminosity feedback possible.

When absolute luminosity measurements are required, values with standard deviations, according to (62), around 7 % are routinely achieved. The error major contributions are due to the ADC system resolution (section 4.1.2) and to the sensitivity of the measurement to the position and crossing angles of the beams at the interaction point (section 4.1.3). Using a larger aperture collimator in front of the calorimeter could reduce the contribution of the second term, but in DAΦNE because of mechanical constraints this cannot be done.

Acknowledgments

The authors want to express their appreciation and thankfulness to O. Coiro, D. Pellegrini, M. Sperati, G. Ceccarelli, L. Iannotti and M. Anelli, for their contribution during the construction of the system. Special thanks are addressed to O. Giacinti for the accurate development of important parts of the monitor electronics. Finally, a sincere gratitude is due to A. Ghigo, A. Drago and G. Di Pirro for their precious collaboration.

Appendix A

Single Bremsstrahlung (SB) Integrated cross-sections.

In reference [7] is reported the SB differential cross-section:

$$\frac{\partial^2\zeta_{SB}}{\partial k\,\partial\cos(\tau)} = 4\alpha r_0^2\frac{m^2}{\omega^2}\frac{1}{k}\left\{\frac{1}{\left[1-\beta\cos(\tau)\right]^2}\left[\frac{\left(\omega^2+\rho^2\right)^2}{\omega^4}-\frac{2\left(\omega^4+\rho^4\right)}{\omega^4}\ln\left(\frac{\omega\rho^2}{2km^2}\right)+\right.\right.$$

$$\left.\left.+\left(\ln\left(\frac{\omega\rho^2}{2km^2}\right)-2\right)\left(\frac{16m^2\rho^2}{\omega^4\left(1-\beta\cos(\tau)\right)}-\frac{32m^4\rho^2}{\omega^6\left(1-\beta\cos(\tau)\right)^2}\right)\right]\right\} \qquad \text{(A1)}$$

where:

$$\rho^2 = \omega^2 - 2\omega k \qquad \text{(A2)}$$

and ζ_{SB} is the SB cross-section, k the SB photon energy in MeV, τ the angle between the SB photon and the emitting particle trajectory, ω the colliding particles total energy in the center of mass system (c.m.s.), β the incoming particle velocity in c units in the c.m.s., m the particle rest mass in MeV, α the fine-structure constant and r_0 the classical electron radius.

In reference [7] is also given the differential cross-section with respect to the photon energy only, obtained by integrating equation (A1) with respect to the emission angle τ:

$$\frac{\partial\zeta_{SB}}{\partial k} = \frac{16}{3}\alpha r_0^2\frac{1}{\omega^2}\frac{1}{k}\left(\omega^2-2\omega k+3k^2\right)\left[\ln\left(\frac{\omega-2k}{2k}\frac{\omega^2}{m^2}\right)-\frac{1}{2}\right] \qquad \text{(A3)}$$

In the case of luminosity measurements using SB photons, it is necessary evaluating the cross-sections integrated within a specified energy range and within a particular solid angle region. For example, by integrating expression (A3) between an energy threshold k_T and the maximum photon energy k_T that a SB photon can have (see expression (2)), it is possible to obtain the cross-section to be used in those luminosity measurements where the detector angular acceptance permits the collection of all the SB emitted photons:

$$\zeta_{SB}(k_T) = 2\alpha r_0^2\left\{\left[-\frac{8}{3}\ln\left(\frac{2k_T}{\omega}\right)-\frac{5}{3}+\frac{16}{3}\frac{k_T}{\omega}-\frac{4k_T^2}{\omega^2}\right]\left[\ln\left(\frac{\omega^2}{m^2}\right)-\frac{1}{2}\right]+\frac{4}{3}\left[\ln\left(\frac{2k_T}{\omega}\right)\right]^2+\right.$$

$$-\frac{2}{3}\left(1-\frac{2k_T}{\omega}\right)\left[\left(\frac{5}{2}-\frac{3k_T}{\omega}\right)\ln\left(1-\frac{2k_T}{\omega}\right)-\frac{7}{4}+\frac{3}{2}\frac{k_T}{\omega}\right]-\frac{16}{3}\frac{k_T}{\omega}\left[\left(1-\frac{3}{4}\frac{k_T}{\omega}\right)\ln\left(\frac{2k_T}{\omega}\right)+\right.$$

$$\left.\left.-\left(1-\frac{3}{8}\frac{k_T}{\omega}\right)\right]-\frac{4}{9}\pi^2-\frac{13}{6}+\frac{8}{3}\sum_{n=1}^{\infty}\left(\frac{2k_T}{\omega}\right)^n\frac{1}{n^2}\right\} \qquad \text{(A4)}$$

In the some more general case, where the angular acceptance of the detector is limited to a maximum angle $\tau_{\max}$, but still in cylindrical symmetry (case of a circular collimator aligned to the beam emitting axis), an analytical expression for the cross section can still be obtained after some algebra:

$$\zeta_{SB}(k_T,\tau_{\max}) = 16\alpha r_0^2 \frac{m^2}{\omega^4}\frac{1}{\beta}\left\{\frac{a_2}{3}\left[\frac{1}{\left(1-\beta\cos(\tau_{\max})\right)^3}-\frac{1}{(1-\beta)^3}\right]+\right.$$

$$\left.+\frac{a_1}{2}\left[\frac{1}{\left(1-\beta\cos(\tau_{\max})\right)^2}-\frac{1}{(1-\beta)^2}\right]+a_0\left[\frac{1}{1-\beta\cos(\tau_{\max})}-\frac{1}{1-\beta}\right]\right\} \qquad \text{(A5)}$$

where

$$a_2 = -32\frac{m^4}{\omega^3}\left[1-\ln\left(\frac{\omega}{m}\right)\right]\left(\frac{\omega}{2}-k_T\right)+16\frac{m^4}{\omega^2}\ln\left(\frac{2k_T}{\omega}\right)\left[\frac{k_T}{\omega}-1+\ln\left(\frac{\omega}{m}\right)\right]+$$

$$+16\frac{m^4}{\omega^3}\left(\frac{\omega}{2}-k_T\right)\ln\left(1-\frac{2k_T}{\omega}\right)-8\frac{m^4}{\omega^2}\left\{\frac{1}{2}\left[\ln\left(\frac{2k_T}{\omega}\right)\right]^2-\frac{\pi^2}{6}+\sum_{n=1}^{\infty}\left(\frac{2k_T}{\omega}\right)^n\frac{1}{n^2}\right\} \qquad \text{(A6)}$$

$$a_1 = -\frac{\omega^2}{2m^2}a_2 \qquad \text{(A7)}$$

$$a_0 = \left(\frac{\omega}{2}-k_T\right)\left[-\frac{3}{2}\omega+4\omega\ln\left(\frac{\omega}{m}\right)+\frac{1}{2}\left(\frac{\omega}{2}+k_T\right)\left(1-4\ln\left(\frac{\omega}{m}\right)\right)\right]+$$

$$+\ln\left(\frac{2k_T}{\omega}\right)\left[-(\omega-k_T)^2+2\omega^2\ln\left(\frac{\omega}{m}\right)\right]+\left(\frac{\omega}{2}-k_T\right)\left(\frac{3}{2}\omega-k_T\right)\ln\left(1-\frac{2k_T}{\omega}\right)+$$

$$-\omega^2\left\{\frac{1}{2}\left[\ln\left(\frac{2k_T}{\omega}\right)\right]^2-\frac{\pi^2}{6}+\sum_{n=1}^{\infty}\left(\frac{2k_T}{\omega}\right)^n\frac{1}{n^2}\right\} \qquad \text{(A8)}$$

If one is interested to the angular dependence of the SB cross-section, the following differential expression can be used:

$$\frac{\partial\zeta_{SB}(\tau,k_T)}{\partial\tau} = -\sin(\tau)16\alpha r_0^2\frac{m^2}{\omega^4}\frac{1}{\left[1-\beta\cos(\tau)\right]^2}\left\{\frac{a_2}{\left[1-\beta\cos(\tau)\right]^2}+\right.$$

$$\left.+\frac{a_1}{1-\beta\cos(\tau)}+a_0\right\} \qquad \text{(A9)}$$

where the a_0, a_1 and a_2 coefficients are still given by the expressions (A6), (A7) and (A8).

Appendix B

Gas Bremsstrahlung (GB) cross-section and detector resolution function

From expression 3CS of reference [9] it is possible to derive the GB differential cross-section to be used in the case of DAΦNE:

$$\frac{\partial \zeta_{GB}(\varepsilon)}{\partial \varepsilon} = \begin{cases} \frac{F_0}{\varepsilon}\left(a\varepsilon^2 - \varepsilon + 1\right) & if \quad 0 \le \varepsilon \le 1 \\ 0 & if \quad \varepsilon < 0, \ \varepsilon > 1 \end{cases} \tag{B1}$$

with the *normalized photon energy*:

$$\varepsilon = \frac{k}{E_0} \tag{B2}$$

and where

$$F_0 = 2Z^2 r_0^2 \alpha \frac{9\varphi_1 - 3\varphi_2 - 8\ln(Z)}{9} \tag{B3}$$

and

$$a = \frac{9\varphi_1 - 12\ln(Z)}{18\varphi_1 - 6\varphi_2 - 16\ln(Z)} \tag{B4}$$

ζ_{GB} is the GB cross-section, k the GB photon energy, E_0 the beam particle energy before the interaction with the gas molecule, Z is the residual gas average atomic number, α is the fine-structure constant and r_0 is the classical electron radius. The quantities φ_1 and φ_2 are constants that can be evaluated in reference [9]. In the case of DAΦNE they assume the values $\varphi_1 = 19.50$ and $\varphi_2 = 19.24$ while $E_0 = 510 \ MeV$. For the residual gas average atomic number it has been used $Z = 6.5$.

Expression (B1) gives the GB cross-section that could be measured with an ideal calorimeter. In the real case the resolution of the detector must be taken into account. Let us consider the case of a detector resolution function (DRF) with gaussian shape and standard deviation given by expression (14):

$$g\left(\varepsilon, \varepsilon_M\right) = \frac{\varepsilon_M^{-1/2}}{\sqrt{2\pi}\ \sigma_{\varepsilon_0}} e^{-\frac{\left(\varepsilon - \varepsilon_M\right)^2}{2\sigma_{\varepsilon_0}^2 \varepsilon_M}} \tag{B5}$$

where σ_{ε_0} is the dimensionless relative resolution that the calorimeter assumes when the particle energy is E_0. At this point, the experimental GB spectrum is obtained by convoluting the convolution between the GB cross-section (B1) with the DRF (B5):

$$\left.\frac{\partial \zeta_{GB}(\varepsilon)}{\partial \varepsilon}\right|_{EXP} = \int_{-\infty}^{\infty} \frac{\partial \zeta_{GB}\left(\varepsilon_M\right)}{\partial \varepsilon} g\left(\varepsilon, \varepsilon_M\right) d\varepsilon_M \tag{B6}$$

or in a more explicit way:

$$\left.\frac{\partial \zeta_{GB}(\varepsilon)}{\partial \varepsilon}\right|_{EXP} = \frac{F_0}{\sqrt{2\pi}\,\sigma_{\varepsilon_0}} \int_0^1 \left(a\varepsilon_M^{1/2} - \varepsilon_M^{-1/2} + \varepsilon_M^{-3/2} \right) e^{-\frac{(\varepsilon-\varepsilon_M)^2}{2\sigma_{\varepsilon_0}^2 \varepsilon_M}} d\varepsilon_M \qquad \text{(B7)}$$

Figure 1 shows the so-called modified spectrum obtained by multiplying expression (B7) by the normalized photon energy ε. Different curves are for different calorimeter resolutions σ_{ε_0}. It can be observed that, independently from the resolution value, all the curves have the same ordinate at the $\varepsilon = 1$ abscissa. This characteristic is used in the calibration procedure described in section 2.2.

References

[1] Zobov M. et al., *Status Report on DAΦNE Performance*, 7th European Particle Accelerator Conference, Vienna June 2000.

[2] Sannibale F. et al., *Luminosity Optimization in DAΦNE*, DIPAC 99, May 16-18, 1999, Chester UK.

[3] Sannibale F. et al., *Beam Measurements for Luminosity Optimization in DAΦNE*, 7th European Particle Accelerator Conference, Vienna June 2000.

[4] Preger M., *A Luminosity Monitor for DAΦNE*, DAΦNE Technical Note IR-3 December 17, 1993.

[5] Potter K., *Luminosity Measurements and Calculations*, Cern Accelerator School, Fifth General Accelerator Physics Course, University of Jyvaskyla, Finland September 7-18, 1992, Vol I pg. 117.

[6] Di Vecchia P., Greco M., *Double Photon Emission in e+ e- Collisions*, Il Nuovo Cimento Vol. L A, N. 2 (July 21, 1967) pg.319.

[7] Altarelli G., Buccella F., *Single Photon Emission in High-Energy e+ e- Collisions*, Il Nuovo Cimento Vol. XXXIV, N.5 (December 1, 1964) pg. 1337.

[8] Dehne H.C. et al., *Luminosity Measurement at ADONE by Single and Double Bremsstrahlung*, NIM 116 (1974) pg. 345.

[9] Koch H. W., Motz J. W., *Bremsstrahlung Cross-Section Formulas and Related Data*, Review of Modern Physics Volume 31, Number 4 (October, 1959) pg. 920.

[10] Boni R. et al., *Operational Experience with the DAΦNE Radio-Frequency Systems*, PAC 1999, New York USA, pg. 866.

[11] Lee-Franzini J. et al., *The KLOE e.m. Calorimeter*, NIM A 360 (1995) pg. 201.

[12] De Zorzi G., Proceedings 4th International Conference on Calorimetry in High Energy Physics, La Biodola, Italy 1993.

[13] Miscetti S., Proceedings 4th International Conference on Calorimetry in High Energy Physics, La Biodola, Italy 1993.

[14] Di Pirro G. Et al., *The Evolution and Status of the DAΦNE Control System*, 7th European Particle Accelerator Conference, Vienna June 2000.

[15] htpp://physics.nist.gov/PhysRefData/Xcom/Text/XCOM.html.